

1 **Protein Assembly Modulation: A New Approach to ALS Therapeutics**

2 Authors

3 Shao feng Yu¹, Kumar Paulvannan¹, Dennis Solas¹, Anuradha F. Lingappa¹, Ana Raquel Moreira¹, Shriya
4 Sahu¹, Maya Michon¹, Danielle Goldsmith¹, Nicholas DeYarman¹, Suguna Mallesh¹, M. Dharma Prasad¹,
5 Claudia Maios², Kai Ruan³ Giulio S. Tomassy^{4,5}, Elizabeth Jensen⁶, Emma McGuirk⁶, Verian Bader⁷,
6 Andreas Mueller-Schiffmann⁷, Jonathan C. Reed⁸, Jaisri R. Lingappa⁸, Vinod Asundi¹, Shi Hong¹, Steve
7 Jacobsen, Lyle Ostrow⁹, Tom Lloyd³, Alex Parker², Kim A. Staats¹⁰, Justin Ichida¹⁰, James Dodge⁶,
8 Debendranath Dey¹, Carsten Korth⁷, Suganya Selvarajah¹, Vishwanath R. Lingappa^{1, 11, 12} and Jeffrey
9 Rosenfeld¹³

10 Affiliations

11 ¹Prosetta Biosciences, Inc. 670 5th St San Francisco, CA 94107

12 ²University of Montreal, Quebec, Canada

13 ³Department of Neurology, School of Medicine, Johns Hopkins University, Baltimore, MD 21205⁴

14 ⁴Biogen, Cambridge, MA 02142

15 ⁵Current affiliation: Sanofi, Genomic Medicine Unit, Waltham, MA 02451

16 ⁶Sanofi, Framingham, MA 01701

17 ⁷Dept of neuropathology, University of Dusseldorf, Germany

18 ⁸ University of Washington, Seattle 98109

19 ⁹ Temple University, Lewis Katz School of Medicine, Philadelphia, PA 19140

20 ¹⁰University of Southern California, Los Angeles, CA 90033

21 ¹¹Department of Physiology, University of California, San Francisco, CA 94116

22 ¹²Corresponding author

23 ¹³ Dept of Neurology, Loma Linda Medical Center, Loma Linda CA 92354

24

25 Abstract

26 Amyotrophic Lateral Sclerosis (ALS) is a neurodegenerative disease with a complex, multifactorial
27 pathophysiology, most commonly manifest as loss of motor neurons. We introduce a new mechanism of
28 ALS pathogenesis via a novel drug-like small molecule series that targets protein disulfide isomerase
29 (PDI) within a previously unappreciated transient and energy-dependent multi-protein complex. This
30 novel drug was found to have activity in cellular models for both familial and sporadic ALS, as well as in
31 transgenic worms, flies, and mice bearing a diversity of human genes with ALS-associated mutations.
32 These compounds were initially identified as modulators of human immunodeficiency virus (HIV) capsid
33 assembly in cell-free protein synthesis and assembly (CFPSA) systems, with demonstrated antiviral
34 activity in cell culture. Their advancement as ALS-therapeutics, and the subsequent separation of activity
35 against HIV and ALS in chemical subseries through structure-activity-relationship optimization, may
36 provide insights into the molecular mechanisms governing pathophysiology of disordered homeostasis
37 relevant to ALS.

38

39

40

41

42

43

44

45

46 Background

47 Aberrant protein aggregation is a common pathophysiologic mechanism implicated in a variety
48 of neurodegenerative disorders (1,2). In the case of ALS, a serious neurodegenerative condition
49 primarily involving motor neurons, it is generally accepted that a cellular manifestation of disease is the
50 mislocalization and aggregation of the protein transactive DNA-binding protein of 43 kDa (TDP-43) (3–8).
51 In healthy individuals, TDP-43 is localized to the cell nucleus (9,10). However, at autopsy, almost all
52 cases of ALS have shown TDP-43 mislocalized to the cytoplasm to varying degrees (5,6,9,10). In these
53 cases, the mis-localized TDP-43 is found in aggregates, typically co-localized with stress-granule proteins
54 (7,11,12). For poorly understood reasons, the end result is selective death of motor neurons.

55 ALS is a challenging disease to study, diagnose, and treat because it is heterogenous in
56 phenotype and progression, both in cells and clinically, in patients (13–15). The overwhelming majority
57 of ALS cases are sporadic, meaning that the ALS patient does not have a clearly identifiable genetic
58 cause or a family history of the disease (16). Among sporadic ALS cases, age of onset, manifestation, and
59 disease progression are variable. While in some cases patient’s symptoms worsen quickly, in another
60 subset they progress slowly (13,15). A small subset of ALS is familial, for which specific gene mutations
61 have been identified (16–18). The proteins encoded by these genes, and those with which they interact,
62 comprise the ALS interactome (5,19). The specifics of how exactly these gene products work together
63 normally, or malfunction to cause ALS, have not been established (20). Likewise, specific toxins have
64 been implicated in the increased incidence of ALS-like syndromes, but their significance for sporadic ALS
65 remains unknown (21).

66 The identification of specific genes in familial ALS has made possible the construction of
67 transgenic animal models that show key phenotypic manifestations of ALS. *Caenorhabditis elegans* is a
68 simple model with a total of 302 neurons (22). The *C. elegans* models for ALS have human TDP-43 or FUS

69 gene mutations or C9orf72 repeat expansions which show neuronal degeneration (23). Wildtype *C.*
70 *elegans* are able to swim in liquid media, but when human ALS-causing mutant transgenic *C. elegans* are
71 placed in liquid medium they display swimming-induced paralysis likely in response to stress (23).
72 *Drosophila melanogaster* is a more complex animal model with nearly three orders of magnitude more
73 neurons (24). *D. melanogaster* with human C9orf72 repeat expansion transgenes show retinal
74 neurodegeneration and developmental lethality (25). Mouse models for ALS, where TDP-43 mutations,
75 C9orf72 repeat expansions, or SOD mutations are introduced as transgenes, show paralysis and
76 neurodegeneration (26).

77 Viral capsid formation is perhaps the most robust protein assembly pathway known(27). Long
78 viewed as occurring through spontaneous self-assembly(28), a body of literature suggests kinetic control
79 over that thermodynamic endpoint of capsid formation through host-mediated catalysis(29–31). We
80 hypothesized that protein aggregation diseases, including ALS, might be related to disordered protein
81 assembly(32). If viral capsid formation is host-catalyzed, then perhaps that is the case more generally for
82 protein assembly. It is only a small further extension of the hypothesis to suggest that protein
83 aggregation diseases reflect dysregulation of a normal catalyzed assembly event. In the case of viral
84 infection the process of repurposing host machinery has been fine-tuned through evolution. In the case
85 of our hypothesis on protein aggregation diseases that process would be more stochastic but once
86 occurring would be just as inexorable. A corollary is that drugs restoring homeostasis by targeting host
87 machinery involved in catalyzed capsid assembly may also be therapeutic for diseases of protein
88 aggregation, such as ALS, if they represent dysfunction of the same or related machinery.

89 We utilized cell-free protein synthesis and assembly (CFPSA) systems to define a catalyzed
90 assembly pathway for viral capsid formation(33,34). That system was then adapted into a moderate
91 throughput drug screen to identify small molecules that block formation of viral capsids (29,30,35,36).
92 We screened a 150,000 compound library for small molecules with protein assembly modulating

93 properties with respect to capsid formation for each of the viral families causing significant human
94 disease, identifying a small numbers of hit compounds for each(27). These “protein assembly
95 modulator” compounds were validated against infectious viruses (29,30,35–37). Subsequently, they
96 were tested in cellular and animal models for nonviral disease, with success (35,37). Data from the
97 application of assembly modulation to oncology indicates that defects in protein assembly are points of
98 overlap in the molecular-level departures from homeostasis that drive progression of both viral and
99 neoplastic disease (35). Treatment with assembly modulators appears to change the composition of
100 particular multi-protein complexes which are comprised of a number of proteins implicated in
101 pathogenesis of the disease, and others implicated in restoration of homeostasis, including through
102 autophagy (35,36). One class of antiviral assembly modulators was shown to target the allosteric
103 regulator 14-3-3 while a second class of assembly modulators with anti-cancer activity was shown to
104 target the allosteric regulator KAP1/TRIM28 (35). We hypothesized that allosteric sites on these catalytic
105 multi-protein complexes could be modulated by our compounds in ways that reverse the disease-
106 associated changes and restore homeostasis, and thereby could have relevance in ALS models
107 associated with aberrant protein aggregation.

108 Applications of these antiviral compounds in the realm of neuroscience in general and ALS in
109 particular, was prompted by two additional considerations. First, that there is a long and enigmatic
110 history of association of particular viruses with specific neurodegenerative diseases. Thus influenza has
111 long been associated with Parkinson’s Disease, herpesvirus infections with Alzheimer’s Disease, and
112 endogenous retroviral activation is observed in ALS (32,38–42). Indeed, the emergence of cognition
113 through natural selection may have been due in substantial measure to retroviral-mediated genetic
114 novelty (43). Second, endogenous retroviral activation has been associated with ALS(42). Together with
115 the forementioned hypothesis that the protein aggregation observed in neurodegenerative disorders
116 may be a variation on the theme of protein assembly, potentially reversible with assembly modulation

117 (32,37), these considerations provided biologically plausible rationales for the line of investigation
118 pursued here. Specifically, in view of these considerations, we used protein assembly modulator
119 compounds active against capsid assembly of retroviruses including HIV as the starting point for our ALS
120 counter screen (30,44). The results, reported here, provide a new framework for understanding the
121 underlying pathophysiology of ALS. We show that a chemical series originally identified and validated
122 against HIV, apparently also corrects a molecular-level defect responsible for TDP-43 mislocalization
123 thereby restoring homeostasis in multiple models of ALS. Importantly, this chemical series can be
124 progressed to a subseries lacking anti-HIV activity with enhanced therapeutic potency for treatment of
125 ALS. Thus, the anti-viral target and the anti-ALS target, while related, appear distinct.

126

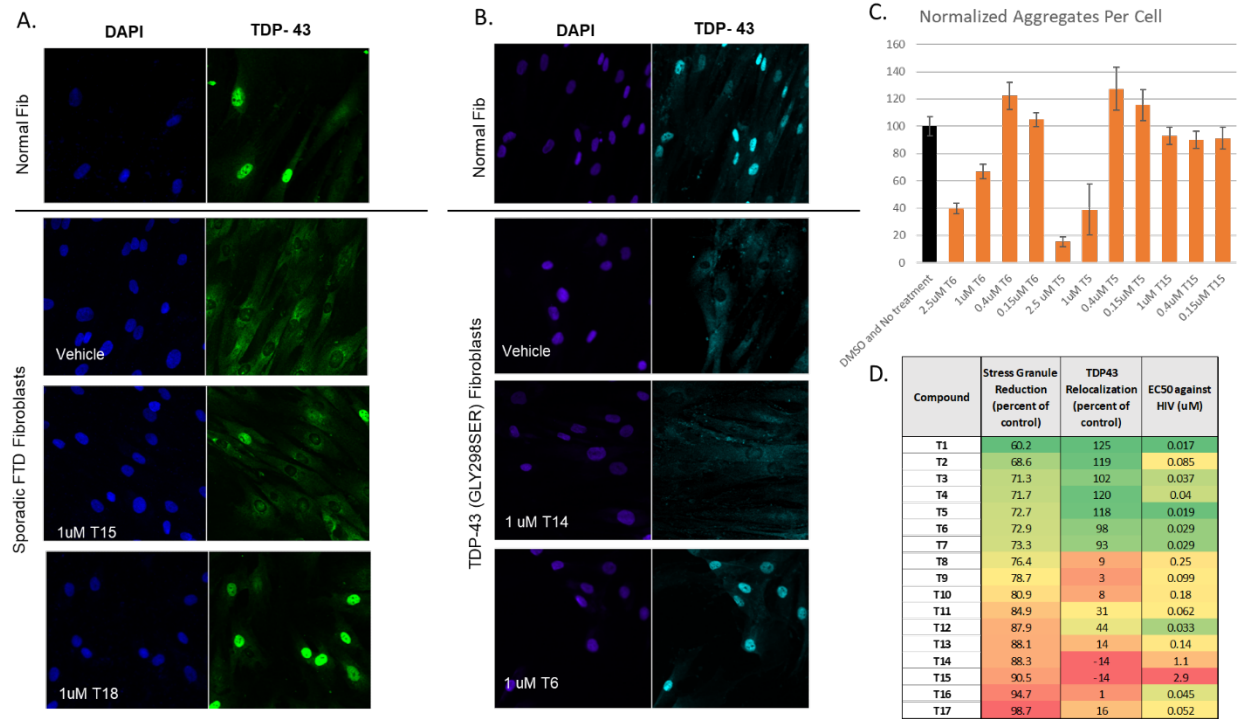
127 Results

128 *Activity of HIV-assembly modulating compounds in cellular models of ALS*

129 A phenotypic screen was established for identifying drug-like small molecule compounds which
130 inhibited HIV capsid assembly in a CFPSA system (30). Hit compounds were termed “protein assembly
131 modulators” due to their observed properties in of blocking capsid formation in CFPSA and cellular
132 systems (30,35,36). The antiviral activity of some hit assembly modulators was validated against
133 infectious HIV in cell culture (30,35). Some validated anti-HIV molecules were members of a
134 tetrahydroisoquinolone (THIQ) chemical series (see **Supplemental Figure 1A** for structure and synthetic
135 scheme of PAV-073, an advanced ALS-selective molecule within this series) (30).

136 Fibroblast cells from patients with familial ALS mutations and from sporadic frontotemporal
137 dementia (FTD) patients, as well as healthy controls, were immunostained for TAR DNA-binding protein
138 43 (TDP-43) which is implicated in both retroviral infection and ALS pathology (36). With high content
139 imaging of these immunostained patient-derived fibroblasts (PDFs), the mislocalization of TDP-43 from

140 the nucleus to the cytoplasm is visible in sporadic, TDP-43 mutant, and VCP mutant fibroblasts, but not
 141 the healthy fibroblasts (see **Figures 1A** and **1B**). The cytosolic TDP-43 could be observed relocalized to
 142 the nucleus upon treatment with active THIQ compounds (see **Figures 1A** and **1B**).



143
 144 **Figure 1. Activity of THIQ assembly modulators in cellular disease models. Figures 1A and 1B** show TDP-
 145 43 mislocalization and relocalization upon treatment with active compounds for PDFs derived from ALS
 146 patients and healthy controls. In the nucleocytoplasmic relocalization assay, cells were seeded and
 147 treated with vehicle or compound for 4 days then washed, fixed, permeabilized and immunostained for
 148 TDP-43 and DAPI. **Figure 1C** shows quantitation of stress granule reduction in PDFs following treatment
 149 with compound. In the stress granule reduction assay, PDFs were treated with compound or vehicle for 24
 150 hours then treated with 500uM sodium arsenite for one hour. Arsenite was washed off and cells were
 151 fixed, permeabilized, and immunostained for TDP-43, Hur, and DAPI. Cell profiler imaging was used to
 152 calculate the number of TDP-43 positive HuR aggregates per cell under each condition and those values
 153 were graphed. **Figure 1D** shows side-by-side comparison of values from the quantitation of the stress
 154 granule reduction assay, the nucleocytoplasmic relocalization assay, and activity against infectious HIV for

155 chemical analogs within the THIQ series. In the infectious virus assay, MT-2 cells were infected with NL4-3
156 Rluc HIV and treated with compound or vehicle for four days. Anti-viral activity is shown as the calculated
157 EC50.

158

159 As a second cellular model for ALS, when PDFs were treated with 500 μ M sodium arsenite for
160 one hour and immunostained, cytoplasmic TDP-43 was found co-localized in stress granules along with
161 HuR (see **Supplemental Figure 2**). Treatment with compounds active in the nucleocytoplasmic assay
162 eliminated the stress granules in a dose-dependent manner (see **Figure 1C**). Following the SAR, most
163 active compounds from the nucleocytoplasmic localization assay also displayed activity in the stress-
164 induced stress granule assay (see **Figure 1D**).

165 The structure activity relationship (SAR) of early compounds from the THIQ series in the
166 nucleocytoplasmic relocalization assay in sporadic FTD fibroblasts generally correlated to their activity
167 against infectious HIV in MT-2 cells (see **Figure 1D**). However, the ALS and HIV activities were separable
168 with further medicinal chemistry advancement, where some analogs (ex. compound T16) showed no
169 TDP-43 relocalization but retained activity against HIV in the nanomolar range, while others (ex.
170 compound T8) showed strong TDP-43 relocalization but substantially weaker antiviral activity compared
171 to other potent compounds (see **Figure 1D**). Similarly, progression of the THIQ lead series resulted in a
172 moderation of toxicity (see **Supplemental Figure 3**). Precisely such a correlation of lowered toxicity to
173 target selectivity for the virally modified multi-protein complex has been observed with lead series
174 advancement for a structurally unrelated respiratory viral capsid assembly modulator(36).

175

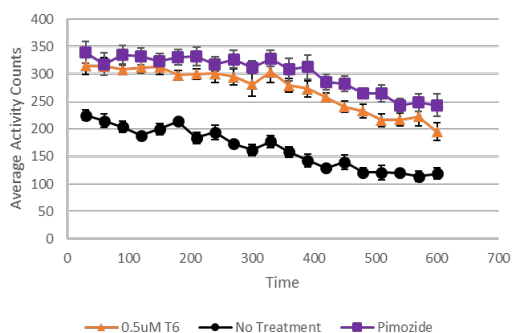
176

177

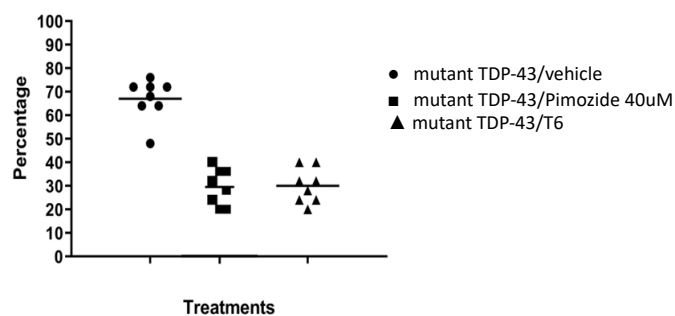
178 *Activity of assembly modulating compounds against animal models of ALS*

179 After achieving efficacy in multiple cellular models for familial and sporadic ALS, we turned to
180 animal models. Lead compounds of the THIQ series were assessed in *C. elegans* with transgenic human
181 ALS TDP-43 A315T mutation. In the swimming induced paralysis (SWIP) assay, transgenic worms were
182 placed in liquid media containing vehicle or compound at a particular concentration. Worms in the liquid
183 media were scored as “paralyzed” if their body cannot make a bending “S” movement. Efficacy was
184 measured as average body bends per second in vehicle-treated versus compound-treated populations.
185 In the neurodegeneration assay, transgenic worms were grown for 9 days and analyzed for motor
186 neuron splits in the presence of vehicle or compound(45)(23). THIQ compounds demonstrated
187 significant reduction of SWIP and long-term neurodegeneration.

A. Activity of T6 in preventing SWIP in mutant TDP-43 Transgenic *C. elegans*



B. Neurodegeneration mutant TDP-43 Transgenic *C. elegans*

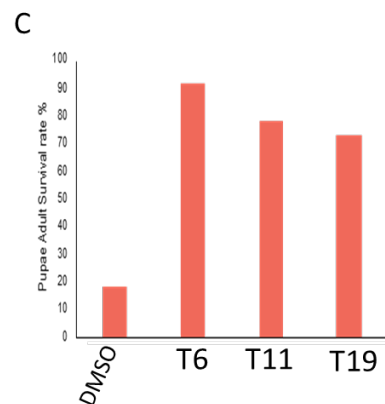
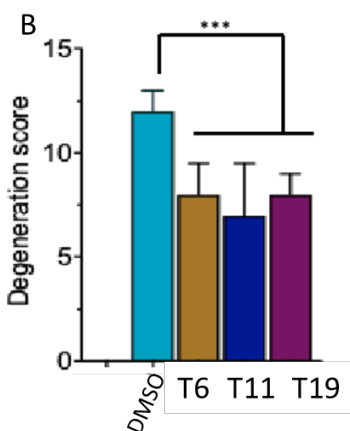
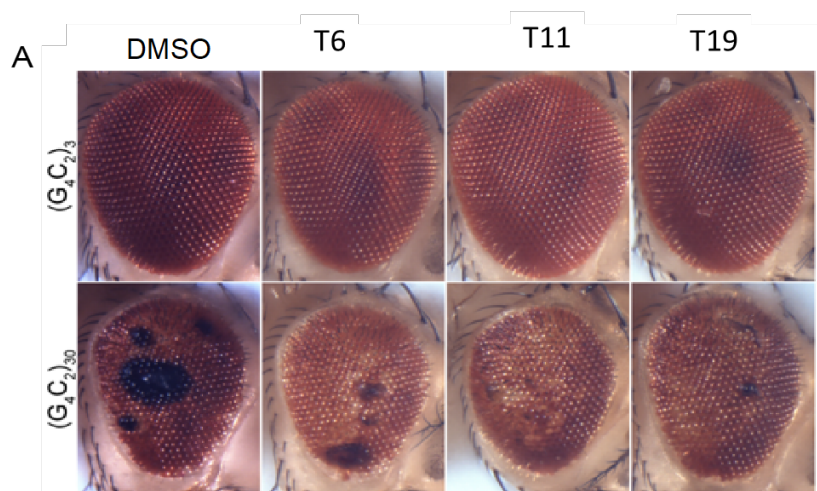


188
189 **Figure 2. Activity in the *C. elegans* model for ALS.** Figure 2A shows rescue of *C. elegans* transgenic for the
190 TDP-43 A315T mutation in the SWIP assay. Worms were grown in the presence of 0.5uM THIQ compound
191 T6, 40uM pimozide, or nothing and movement was recorded by video. The experiment was performed in
192 8 replicates of 25 worms each and the average number of body bends per second is shown for each
193 condition. Figure 2B shows rescue of *C. elegans* transgenic for the TDP-43 A315T mutation in the long
194 term neurodegeneration assay. Worms were grown in the presence of 0.5uM THIQ compound T6, 40uM

195 pimozide, or vehicle for 9 days and analyzed for motor neuron splits. Percentage of neurons showing
196 splits is shown for each condition.

197

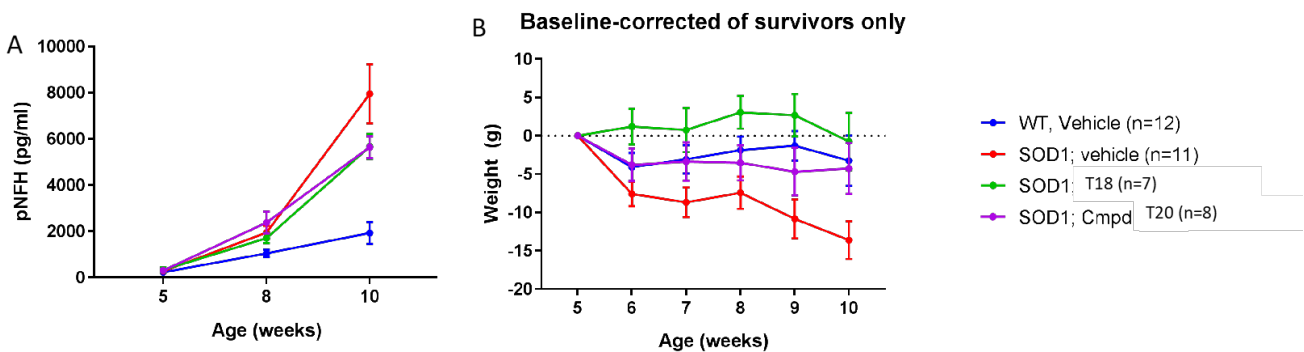
198 Active compounds from the series were then assessed in *D. melanogaster* transgenic for the
199 C9orf72 30 G4C2 repeat expansion. Overexpression of 30 G4C2-repeats in fly motor neurons using
200 OK371-GAL4 causes lethality due to paralysis, preventing the exclusion of the adult from the pupal case.
201 Treatment significantly reduced lethality and degeneration caused by 30 G4C2 repeats than when
202 compared with DMSO vehicle alone.



203

204 **Figure 3. Activity in the *D. melanogaster* model for ALS.** THIQ compounds T6, T11, and T12 were tested
205 alongside vehicle in wildtype and transgenic *D. melanogaster* overexpressing C9orf72 30 G4C2. **Figure 3A** shows
206 images of degeneration (black spots) in drosophila eye for wildtype (top row) and transgenic (bottom row)
207 animals. **Figure 3B** shows the corresponding quantitation for degeneration observed in drosophila eye. **Figure 3C**
208 shows percent adult survival in vehicle versus compound treated conditions.

209 We then wanted to assess activity in a mouse model. Vehicle or compound was administered to
210 mice transgenic for the SODG93A mutation every day for 5 weeks (beginning when the mice were 5
211 weeks old) by intraperitoneal (IP) dosing. Vehicle was also administered by IP to wildtype mice as a
212 control. Both test compounds showed significant, positive results based on biochemical data (levels of
213 phosphorylated neurofilament heavy chain subunit measured in plasma) and clinical criteria (prevention
214 of weight loss).



215 **Figure 4. Activity in the SOD1 mouse model for ALS.** THIQ compounds T18 and T20 were tested alongside
216 vehicle in transgenic mice expressing the SOD G93A mutation. **Figure 4A** pNFH and **Figure 4B** shows
217 weight over the course of the study with significant improvements in the compound-treated animals.
218 Error bars represent standard deviation.

220

221 *Target identification in ALS and FTD patient fibroblasts and mouse brain samples*

222 Previous studies on protein assembly modulator small molecule mechanism of action has shown
223 that they target dynamic multi-protein complexes, a feature which appears shared by structurally-
224 unrelated assembly modulator chemotypes efficacious in other therapeutic areas (35,36). The formation
225 and action of these multi-protein complexes appears to be dependent on metabolic energy (nucleotide
226 triphosphate hydrolysis). Protocols for energy-dependent drug resin affinity chromatography (eDRAC)
227 provided a method to characterize the targets of assembly modulating compounds (35,36). In those
228 experiments, extract from a disease-relevant cell line or tissue sample would be incubated with a
229 modified analog of a compound attached to an Affi-gel resin and serve as an affinity ligand for target
230 identification (46). The eDRAC experiments made possible tandem mass spectrometry (MS-MS)
231 determination of protein composition of the isolated target multi-protein complexes under various
232 conditions including healthy versus disease cells/tissues, with and without metabolic energy
233 supplementation, and under vehicle versus compound treatment conditions (35,36). We sought to apply
234 the same techniques to the ALS-active assembly modulators in order to better understand their targets
235 and mechanism.

236 Cellular extract was prepared from the brain tissue of a wildtype mouse and a transgenic mouse
237 expressing the SOD1 G93A mutation. Extract was supplemented with an “energy cocktail” of
238 ribonucleotide triphosphates (to a final concentration of 1mM rATP, 1mM rGTP, 1mM rCTP, 1mM UTP),
239 creatine phosphate, and 5 ug/mL creatine kinase. Extract was incubated on an Affi-gel resin coupled to a
240 compound from the THIQ series which exhibited potent activity in both SGA, NCA, or a control resin
241 which consisted of an affi-gel matrix couple to itself, for an hour at 22°C (30). The resins were washed
242 with 100 bed volumes of buffer and eluted with 100 uM compound containing the energy cocktail first
243 for two hours at 22°C, and then a second eluate collected overnight, followed by stripping the column
244 with SDS. The overnight eluate was analyzed by MS-MS. 166 proteins were identified by spectral count

245 in the wildtype eDRAC eluate (see **Figure 5A**). 208 proteins were identified by spectral count in the SOD1
 246 eDRAC eluate (see **Figure 5A**).

247

248

249

250

251

252

253

254

255

256

257

258

259

260

261

262

263

A

Protein	Wildtype Mouse Brain on Control Resin	Wildtype Mouse Brain on THIQ Resin	SOD1 Mutant Mouse Brain on Control Resin	SOD1 Mutant Mouse Brain on THIQ Resin	Protein	Wildtype Mouse Brain on Control Resin	Wildtype Mouse Brain on THIQ Resin	SOD1 Mutant Mouse Brain on Control Resin	SOD1 Mutant Mouse Brain on THIQ Resin
1433E	0	0	0	4	MAP1B	0	5	0	10
1433G	0	5	0	7	MAP6	0	6	0	9
1433T	0	0	0	4	MARCS	0	0	0	2
1433Z	0	0	0	4	MBP	8	15	11	14
2A5B	0	0	0	2	MET2	0	2	0	2
2AAA	0	16	0	16	MK01	0	5	0	7
ACAD8	0	2	0	0	MK03	0	3	0	7
ACBG1	0	0	0	3	MMSA	0	0	0	3
ACLY	0	0	0	4	MDES	2	2	2	3
ACD11	0	4	0	4	MIPR	0	3	0	4
ACTG	5	32	10	30	NAKD2	0	7	0	6
ACTN4	0	4	0	4	NCAM1	0	10	0	16
ACTZ	0	0	0	3	NDKA	0	2	0	0
ADP1	0	0	0	3	NDRG2	0	16	0	17
AL1A1	0	3	0	4	NDRG4	0	4	0	0
AMRP	0	2	0	0	NDUF2	0	0	0	0
ANXA2	2	0	2	0	NEDD4	0	2	0	3
AP2A2	0	0	0	2	NRCAM	0	3	0	4
AP2B1	0	0	0	2	NSF	0	5	0	6
AP2M1	0	0	0	3	NSFC	0	0	0	2
AT1A1	0	15	0	20	NUCB1	0	7	0	7
AT1A2	0	20	0	25	ODO1	0	7	0	8
AT1A3	0	23	0	31	ODO2	0	3	0	2
AT1B1	0	3	0	3	OOPB	0	0	0	2
AT1B2	0	4	0	4	P5CR3	0	0	0	2
AT2A2	0	2	0	4	PCBP1	0	0	0	2
AT2B1	0	0	0	13	PCSK1	2	7	0	8
AT2B2	0	12	0	27	PDIA1	0	4	0	13
ATSF1	0	2	0	0	PGTA	0	0	0	4
ATPH	0	0	0	3	PHIP	0	3	0	4
ATPA	0	24	0	13	PLAK	0	0	3	0
ATPB	0	29	0	23	PP2A	0	4	0	5
ATPG	0	4	0	2	PP2A8	0	12	0	18
BACH	0	3	0	2	PP2B8	0	6	0	12
CADW3	0	3	0	4	PRDX1	0	8	0	9
CALM1	0	13	0	13	PRDX2	0	7	9	9
CALX	0	2	0	3	PRDX3	0	8	0	7
CAP51	0	0	0	2	PRDX6	0	0	0	2
CATA	0	0	0	2	PRT2	0	3	0	3
CATD	0	2	0	4	PSD12	0	0	0	2
CCO22	0	2	0	0	PSMD3	0	0	0	2
CEND	0	2	0	2	PSMD6	0	0	0	3
CH60	0	39	0	42	PYC	0	9	0	11
CN37	0	7	0	10	PYGB	0	39	0	45
COA7	0	2	0	2	PYGM	0	46	0	42
COQ9	0	2	0	3	RAB3A	0	2	0	3
COMC	0	0	0	2	RABE1	0	2	0	3
CPLX1	0	8	0	7	RP3A	0	0	0	2
CPLX2	0	0	0	8	RT36	0	3	0	3
CSN4	0	2	0	3	RTN1	0	5	0	7
CSRP1	0	3	0	0	RTN3	0	0	0	4
CYB5	0	2	0	2	RTN4	0	2	0	5
DC111	0	2	0	5	RYR1	0	2	0	0
DC112	0	0	0	7	SAP	0	2	0	0
DC113	0	2	0	3	SC23A	0	2	0	3
DC12	0	4	0	5	SDHA	0	4	0	2
DISP	4	4	13	3	SEB1	0	3	9	12
DHEH	0	21	0	16	SEPT7	0	0	0	4
DLDH	0	3	0	2	SEP11	0	0	0	4
DLRB1	0	2	0	0	SHLB2	0	0	0	3
DMXL2	0	0	0	3	SR2	0	10	0	7
DNM2	0	0	0	2	SNB3	0	0	0	5
DPLX2	0	6	0	7	SNAG	0	0	0	4
DYH1C1	0	14	0	16	SNP25	0	6	0	8
DYL2	0	2	0	0	SPN90	0	2	0	0
E41L3	0	2	0	3	SPTR2	0	2	0	0
EAA1	0	6	0	8	SPTN1	0	8	0	8
EAA2	0	2	0	4	STP1	0	4	0	15
ECHA	0	2	0	0	STX1B	0	12	0	13
EF1A1	0	10	0	11	STXB1	0	19	0	30
EF1G	0	5	0	4	SUCB1	0	0	0	2
EFTU	0	0	0	3	SYK	0	2	0	0
EPH1	0	0	0	2	SYNL	0	0	0	3
F10A1	0	7	0	5	SYN2	0	8	0	10
FAS	0	2	0	4	SYPH	0	0	0	2
FKB1A	0	2	0	0	SYUA	0	0	0	2
FSP2	0	0	2	0	SYUB	0	5	0	5
FUBP1	0	4	0	2	SYUG	3	2	3	4
FUBP2	0	4	0	6	SYWC	0	0	0	2
G3P	0	21	2	24	TBA1A	0	33	4	35
GBB1	0	3	0	3	TBA4A	0	30	0	33
GBB2	0	3	0	4	TBB2A	0	42	0	49
GLNA	0	4	0	4	TBB3	0	38	0	41
GLSK	0	15	0	17	TBB4A	0	43	0	46
GNAO	0	6	0	8	TBB4B	0	43	0	48
GPM6A	0	4	0	6	TBB5	0	41	0	47
GPM6B	0	2	0	2	TCPA	0	9	0	5
GRP75	0	3	0	8	TCPB	0	11	0	12
GRP78	0	6	0	9	TCPD	0	5	0	5
GSTM1	0	4	0	4	TCPE	0	10	0	9
GSTP1	0	2	0	0	TCPG	0	8	0	5
H13	7	7	11	10	TCPH	0	2	0	2
H14	8	9	10	11	TCPQ	0	7	0	7
H2A2C	5	3	3	3	TCPZ	0	3	0	3
H2B1M	8	7	10	10	TIBA	0	34	0	41
H2B3B	0	0	9	0	TM13	0	0	0	2
H3C	4	4	4	4	TPM2	0	0	0	4
H4	4	6	5	8	TPM3	0	0	0	3
HBA	5	14	5	12	TYCL	0	0	0	2
HBB1	0	10	2	8	TYL10	4	4	4	4
HEMH	0	0	0	2	TYB4	6	5	6	5
HMGB1	8	14	8	11	UBB	3	0	4	3
HNHR2	0	0	0	3	UBP5	0	0	0	8
HS90A	0	0	0	17	USO1	0	2	0	3
HS90B	0	12	0	20	USP9A	0	0	0	12
HSP7C	0	32	0	37	VAMP1	0	2	0	0
IDH3A	0	0	0	2	VAMP2	0	3	0	2
IMB1	0	0	0	2	VAT1	0	13	0	7
ITSN1	0	0	0	3	VATA	0	12	0	16
KCC4	0	0	0	3	VATB2	0	8	0	12
KIF5C	0	0	0	3	VATE1	0	4	0	5
LIN7C	0	0	0	3	VATG2	0	7	0	8
LMNA	0	2	0	0	VIME	0	5	6	0
LRP1	0	0	0	3	VINC	0	2	0	0
LYZ1	0	2	0	0	WDR7	0	0	0	3
MAP1A	6	0	0	7					

264

265

266

267

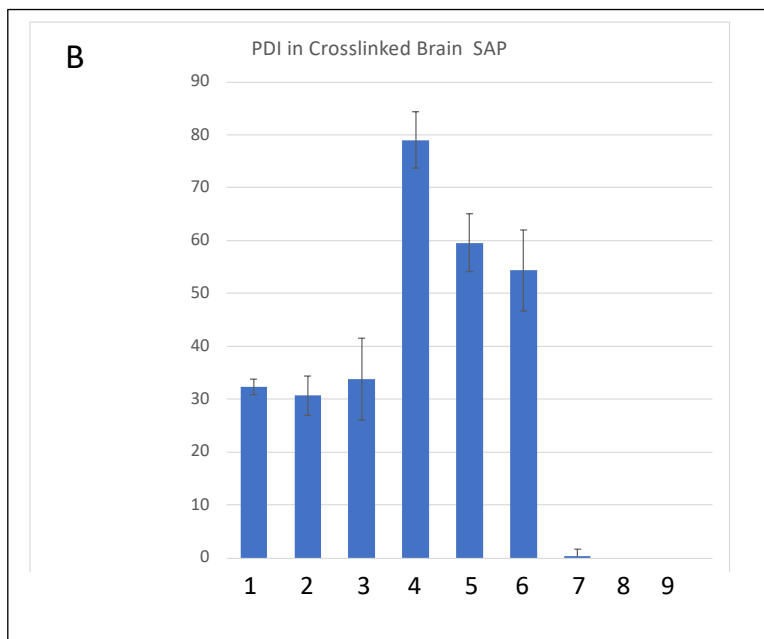
268

269

270

271

272



273

274

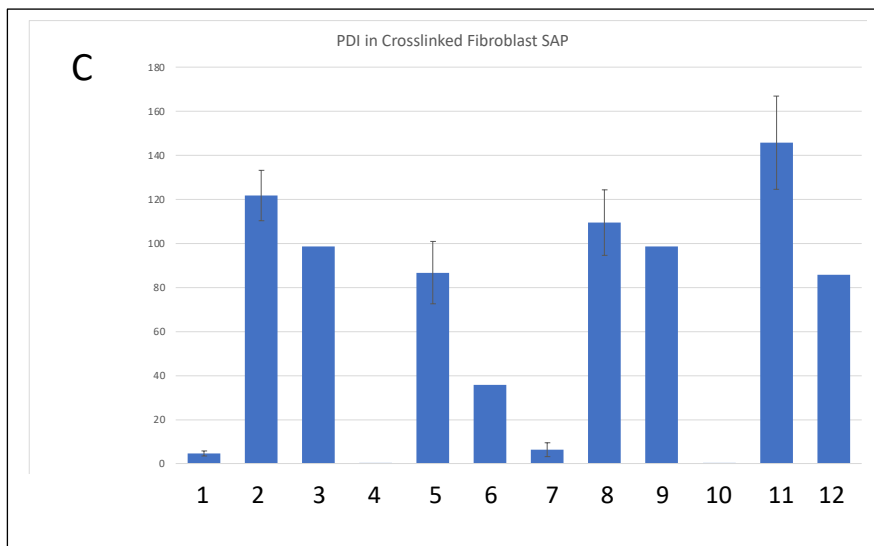
275

276

277

278

279



280

281

282

283

284

Figure 5. Target identification in mouse brain and PDF samples. Figure 5A shows MSMS analysis of the eDRAC eluate from a THIQ resin (30). Healthy wildtype or sick SOD1 G93A mutant mouse brain which was incubated on the THIQ resin or a control resin (affigel lacking the attached drug), washed and eluted with free compound, with the eluates analyzed by MS-MS. A list of proteins identified, and the number of spectral counts detected for each starting material and resin is shown where conditional formatting has

285 been applied on a red-to-green scale. Protein disulphide isomerase (PDI) is detected in both drug resin
286 eluates, but not the control resin eluates. Figure 5B shows the results of a photocrosslinking study in
287 which healthy (bars 1, 4, 7), sick SODG93A (bars 2, 5, 8) or sick-THIQ-treated (bars 3, 6, 9) mouse brain
288 was assessed with PAV-073 crosslinker under native (bars 1-3) or denatured (bars 4-6) conditions. Bars 7-9
289 show that addition of excess free drug during the crosslinking reaction eliminates PDI precipitation. This
290 demonstration of competition between free drug and the photocrosslinker is an important line of
291 evidence that the modification of structure occurring during crosslinker construction did not alter the
292 capacity for target engagement. In Figure 5C photocrosslinking is done with healthy (bars 1-6) versus ALS
293 PDF extracts (bars 7-12) handled in much the same way as in Figure 5B (native SAP bars 1-3 and 7-9;
294 denatured bars 4-6 and 10-12), except that an additional control was performed in which crosslinker-
295 biotin lacking the drug was shown not to precipitate PDI (bars 1, 4, 7, 10). Free drug competitor is shown
296 in lanes 3, 6, 9, 12). For both 5B and 5C after crosslinking, the samples were divided in two, one of which
297 was denatured in 1% SDS at 100°C for 3 minutes before addition of excess non-denaturing detergent
298 (Triton-X-100) to take up the free SDS into micelles. Streptavidin beads were added and the bound protein
299 was precipitated and analyzed by western blot. Quantitation of the protein band for PDI is shown as
300 arbitrary density units, where error bars represent the averages of triplicate-repeated conditions.

301
302 To determine which of the proteins detected in the eDRAC eluate directly binds to the
303 compound, a photocrosslinker compound was synthesized in which diazirine and biotin moieties were
304 attached at the same position used previously to attach to the resin. Thus, upon exposure to UV light, a
305 covalent bond is formed between the diazirine moiety of the compound and the nearest neighbor
306 protein. Under native conditions (in the presence of metabolic energy) the full complex is isolated.
307 However upon denaturation, followed by streptavidin precipitation (SAP), only the nearest neighbor
308 drug-binding protein, to which an irreversible covalent crosslink has been achieved, is recovered and is
309 identifiable by western blotting.

310 Compound PAV-073 was chosen as the analog to be used as a photocrosslinker for the THIQ
311 series because its activity is selective to ALS, having largely lost efficacy against infectious HIV (see
312 **Supplemental Figure 1** for activity of PAV-073 and **Supplemental Figure 4** for synthetic scheme of PAV-
313 073 crosslinker). Crosslinking and SAP from mouse brain extract (brains from the SODG93A efficacy
314 study, including wildtype, transgenic mutant, and transgenic mutant/compound treated animals)
315 identified protein disulphide isomerase (PDI) as a direct target . Western blot analysis showed a protein
316 band for PDI present in both native and denatured samples when crosslinked with PAV-073 but not the
317 negative control (see **Figure 5B**). Furthermore, the PDI band was diminished with presaturation, where
318 the free PAV-073 was added to the sample before crosslinking to compete out binding-sites (see **Figure**
319 **5B**).

320 The crosslinking experiment was repeated using cellular extract prepared from a sporadic ALS
321 patient (#51) and healthy control (#27) fibroblasts (see **Figure 5C**). For both PDF and brain samples, PDI
322 was present as a target in both healthy and ALS conditions in eDRAC and crosslinking (See **Figures 5A-C**).

323

324 Discussion

325 The protein assembly modulator THIQ chemotype which is shown here active in a diversity of
326 ALS cellular and animal models, appears to work for both familial and sporadic cases based on data
327 shown here, generated in ALS patient-derived fibroblasts and transgenic worms, flies, and mice. Activity
328 of hit compounds appears to normalize an array of surrogates for ALS pathology including elimination of
329 stress-induced TDP-43 aggregates in stress granules, repair of TDP-43 mis-localization, reversal of
330 paralysis, reversal of neurodegenerative markers, normalization of weight, and increased lifespan.
331 Compounds appeared active on models for VCP, TDP-43, C9orf 72, and SODG93A mutations. This is
332 consistent with an expectation that protein assembly modulation is an upstream manipulation that

333 serves to integrate multiple biochemical pathways and thus is therapeutic for a wide range of
334 downstream defects.

335 The premise in support of our unconventional approach to drug discovery and our pivot from
336 focusing on viral to nonviral diseases once hit compounds were identified, was that viruses have used
337 deep evolutionary time and natural selection to find the most efficient ways to take over our cells and
338 prevent activation of host defensive measures. Thus viral targets discovered via host-viral interactome
339 pathways likely represent weak links of human biology at risk for diseases involving departures from
340 homeostasis- including those not caused by viruses. Experimental data appears to support this
341 hypothesis as assembly modulator compounds have shown distinctive activity against viral disease(36),
342 proliferative disease(35), and for neurodegenerative disease both for ALS as presented here, and
343 previously for Alzheimer’s Disease (47).

344 Our findings should not be misunderstood as suggesting that viruses are causative of the
345 neurodegenerative diseases including ALS with which they are associated. Rather our data suggest a
346 shared molecular consequence of both viral infection and ALS: disruption of homeostasis. The data
347 presented here suggests that this occurs by a specific molecular mechanism that involves critical
348 components of protein assembly that can be manipulated with allosteric site-targeted protein assembly
349 modulator drugs, to therapeutic advantage. In the case of viruses manipulation of protein assembly
350 blocks viral capsid formation and restores the normal function of a repurposed host multi-protein
351 complex (36). In the case of ALS a related but distinct multi-protein complex is targeted, as shown here.
352 The precise similarities, differences, and relationship of the viral and ALS targets, and the relationship of
353 healthy to aberrant forms occurring in disease, remains to be further studied. However the therapeutic
354 consequences of these manipulations as shown here, suggests this to be a productive path for future
355 effort.

356 We have observed that, for multiple areas of disease and multiple classes of chemical
357 compounds, protein assembly modulators target dynamic multi-protein complexes via a protein
358 implicated in allosteric regulation. One chemotype series active against all respiratory viruses
359 accomplishes this by targeting 14-3-3 proteins (36,48). Another chemotype active against cancer targets
360 KAP1 (35,49). The Alzheimer's Disease assembly modulator targets MIF (47). The ALS/HIV active
361 chemotype described in this paper targets PDI, a protein also implicated in allosteric regulation and in
362 cleavage of disulfide bonds (50–53). Variants of PDI with single nucleotide polymorphisms and
363 redistribution of PDI within different regions of the cell, including endoplasmic reticulum sub-
364 compartments, are implicated in the literature as correlating with ALS symptoms(54–56). Furthermore,
365 expression of PDI has been observed to protect mice against neurodegeneration in the SOD1G93A
366 model as well as multiple cellular models of ALS (55,57–59). The PDI detected in the compound's target
367 by eDRAC of both healthy and ALS patient fibroblast cells, appears to be interacting with other proteins
368 in a similarly energy-dependent manner as the other assembly modulator compounds described (35,36).
369 As for the other assembly modulators, the protein composition of the multi-protein complex drug target
370 differs between healthy and sick cells (Figure 5A), although we do not yet have compelling evidence, as
371 observed for other assembly modulators(36), for normalization of a disease-associated target. Possible
372 explanations include the need to continue to drive SAR further towards disease-selectivity, that the
373 specific allosteric site targeted is shared by both healthy and sick individuals with disease-specific
374 features not reflected in the analysis to date.

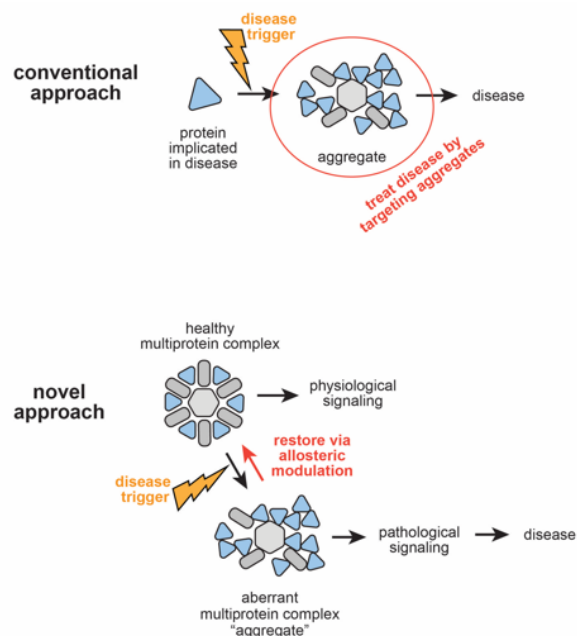
375 We hypothesize that the unique properties observed in multiple distinct chemical classes of
376 assembly modulators may be attributable to their having a mechanism of action that works via allosteric
377 regulation. Targeting allosteric sites instead of active sites may be an effective strategy to selectively
378 inhibit activity of the subsets of proteins which have been dysregulated in a diseased state, without
379 targeting the forms in the healthy state. Modulation of the multi-protein complex that catalyzes protein

380 assembly may provide a means of restoring homeostasis, rather than simply blocking a disease-
381 associated form, without restoration of homeostasis.

382 Our use of viral assembly as a surrogate for discovery of small molecule protein assembly
383 modulators of relevant allosteric sites for the restoration of homeostasis has proven productive. In part,
384 this may be because it is not constrained by the limitations of current technology. Identifying allosteric
385 sites, which affect activity of a small subset of a given gene product cannot be easily achieved through
386 genetic manipulation, given the evidence for protein “moonlighting”(60,61). Of necessity, genetic
387 manipulation affects all of the diversity of forms of a particular gene product, irrespective of the
388 different functional roles they may play. Since only one of these functions may be responsible for the
389 disease, targeting all forms and their functions, may obscure therapeutic effect, e.g. through off-target
390 liabilities. Finding a small molecule that selectively targets only the relevant subset of protein-protein
391 interactions provides a path to retain broad activity while avoiding toxicity, as demonstrated for other
392 protein assembly modulator compounds(35,36), and suggested for ALS from the data presented here.

393 Efficacy of the same protein assembly modulator small molecule in both familial and sporadic
394 ALS supports the hypothesis that these compounds act on an upstream regulatory mechanism rather
395 than on downstream consequences of disease (manifest as protein aggregates). Thus one therapeutic
396 small molecule is broadly applicable despite the heterogeneity of ALS. As an analogy, when car crashes
397 frequently occur at a busy intersection, upstream solutions, like installing a stop sign or fixing a broken
398 traffic light, are more effective than a focus on downstream consequences, such as sending more tow
399 trucks to remove roadside wreckage. Sending tow trucks to remove the wreckage will improve traffic in
400 the short term, but if the underlying defect which led to the crash is not addressed— it is only a matter
401 of time before it happens again. Targeting the aggregates themselves is akin to eliminating wreckage
402 solely by sending tow trucks following a crash. Allosteric modulation on the other hand, is a way to
403 prevent wreckage by installing a stop sign to regulate traffic from a distance(62). Figure 6 illustrates the

404 distinction between conventional thinking with regards to protein aggregate-associated diseases
405 including ALS, and the hypotheses formulated and tested here.



406
407 **Figure 6. Protein assembly modulation drug action.** Hypothesized mechanism of protein assembly
408 modulator drug action for protein aggregation diseases including ALS, based on the data. Top:
409 conventional approaches aimed at removal of aggregates. Bottom: Protein assembly modulation
410 approach to preventing aggregate formation. By targeting an allosteric site to prevent aggregate
411 formation, rather than targeting aggregates after they have formed, the outcome is akin to installing a
412 stop sign to prevent accidents at a busy intersection, rather than sending tow trucks to remove wreckage
413 once an accident has occurred.

414
415 Another implication of the findings presented here is that, though the targets of the viral and
416 related non-viral diseases are similar, they are nevertheless sufficiently distinctive that their activity can
417 be separated through SAR advancement. We observed early compounds in the THIQ series show
418 potency in models for both ALS and HIV. However, the advanced ALS-active compound PAV-073,

419 demonstrated potent activity in the worm model for ALS while showing substantial loss of activity
420 against infectious HIV in cell culture. Not shown, a different advanced subseries is HIV-selective, without
421 activity in an ALS model. This suggests that there are two separate targets (one relevant for ALS, one for
422 HIV) for this chemical series. Driving the SAR towards selectivity will likely diminish liability for off-target
423 toxicity and illuminate the molecular mechanisms underlying each disease state in ways that have been
424 heretofore inaccessible.

425

426

427

428

429

430

431

432

433

434

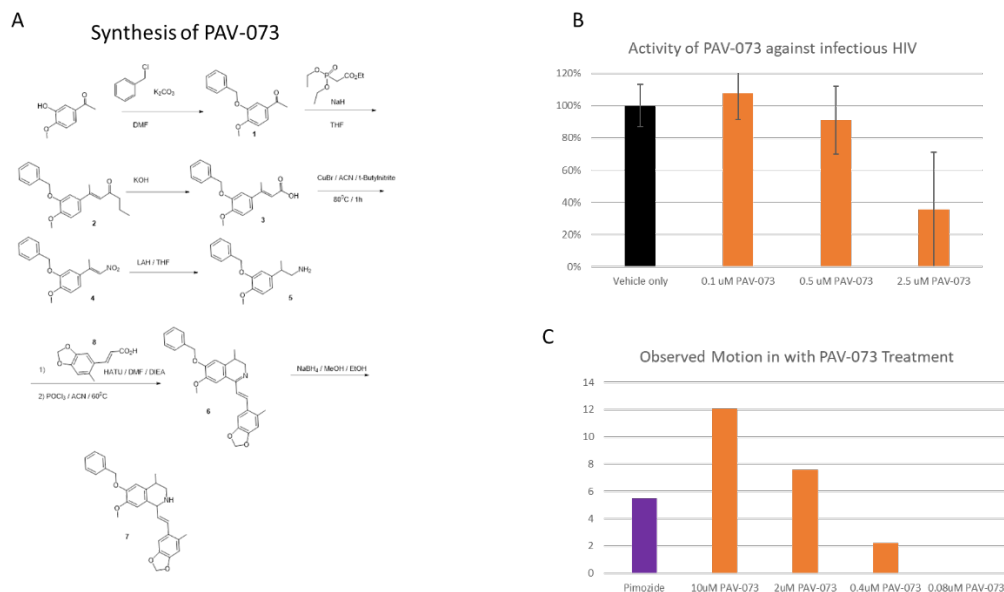
435

436

437

438

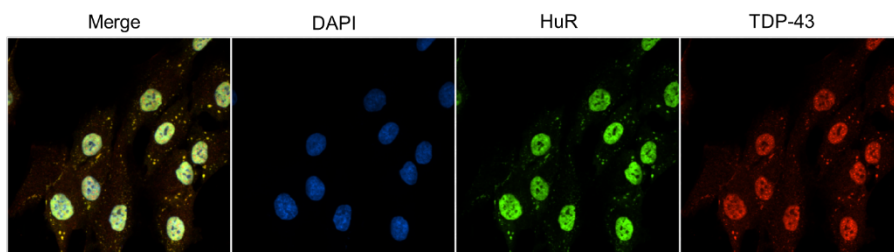
439 Supplemental Figures



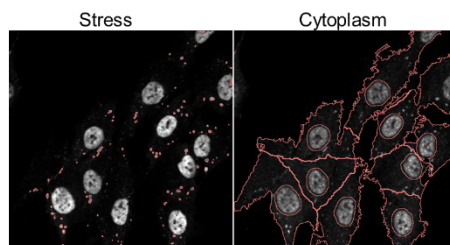
440

441 **Supplemental Figure 1. Synthesis and activity of PAV-073.** Supplemental Figure 1A shows the synthetic
442 scheme for PAV-073. Supplemental Figure 1B shows activity of PAV-073 against infectious HIV. MT-2 cells
443 were infected with NL4-3 Rluc HIV and treated with PAV-073 for four days. Averages and standard
444 deviation of viral titer observed with triplicate repeated dose-titrations of PAV-073 are shown as a
445 percentage of the titer observed in DMSO-treated cells. Supplemental Figure 1C shows activity of PAV-
446 073 relative to pimoizide (40uM) in ameliorating the condition of transgenic *C. elegans* expressing the
447 human TDP-43 A315T mutation. Nematodes were age-matched and grown on standard nematode grown
448 media plates until day 1 of adulthood at which point they were collected and placed in 96 well plates (50-
449 70 animals per well) and treated with compound or control. Animal movement was then tracked for 30
450 minutes using WMicroTracker ONE.

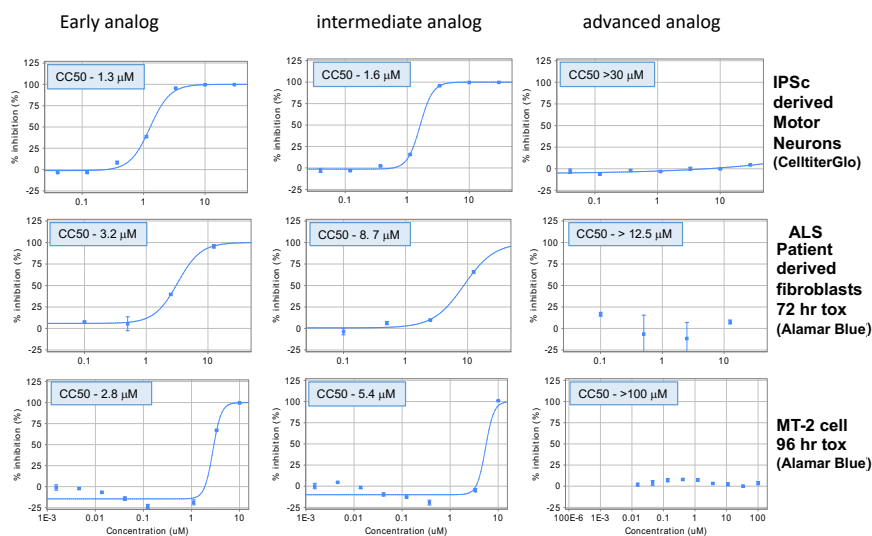
A Sporadic FTD Patient Fibroblast treated with 500 μ M Sodium Arsenite for 60 mins and Analyzes by Cell Profiler



B Identification of cytoplasm HuR and TDP-43 aggregates by Cell Profiler



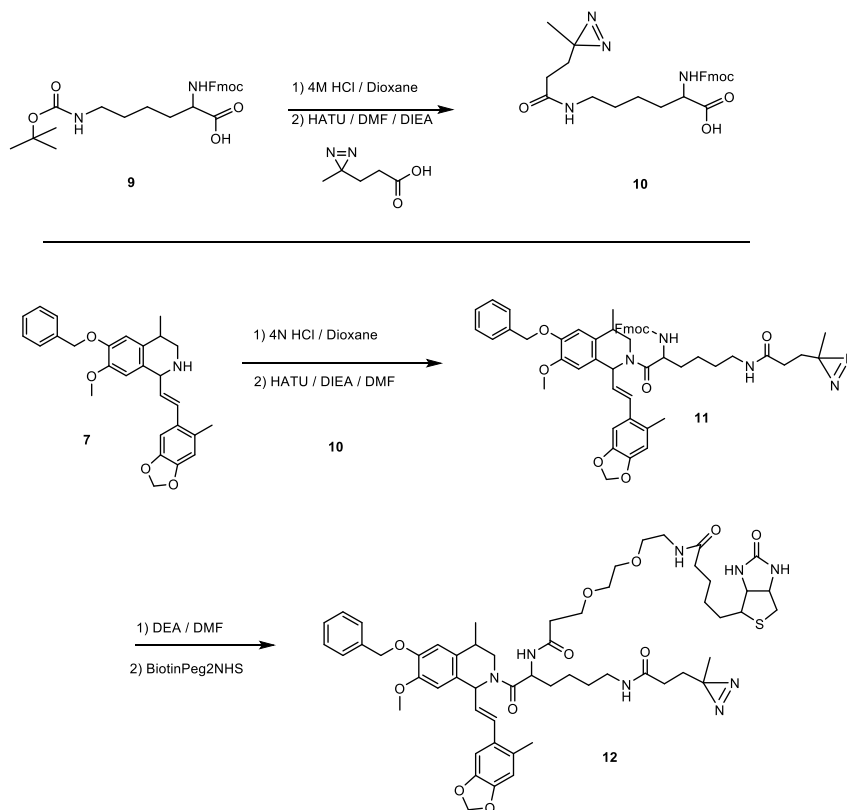
451
452 **Supplemental Figure 2. Stress granule induction and quantitation. Supplemental Figure 2A shows**
453 **immunostain for DAPI, HuR, and TDP-43 in PDFs treated with 500uM sodium arsenite for one hour. Figure**
454 **2B shows how cell profiler imaging was used to identify the number of TDP-43 positive HuR aggregates**
455 **per cell.**



456
457 **Supplemental Figure 3. Moderation of toxicity with THIQ lead series advancement. Compounds of**
458 **comparable potency but differences in toxicity were identified from the lead series and assessed**
459 **in transformed cells, ALS PDFs, and iPSC-derived motor neurons. The lead series progression**

460 to diminished toxicity is confirmed in all cell lines using both cell TiterGlo and Alamar Blue
461 toxicity assays.

462



463

464 **Supplemental Figure 4. Synthetic scheme for PAV-073 photocrosslinker analog. Supplemental Figure 3**

465 shows the synthetic scheme for the photocrosslinker analog of PAV-073 used to identify PDI as the direct

466 drug binding protein (see **Figure 5**).

467

468

469

470

471 Materials and Methods

472 **Lead contact and Materials Availability**

473 Further information and requests for resources and reagents should be directed to and will be fulfilled
474 by the Lead Contact Vishwanath R. Lingappa (vlingappa@prosetta.com).

475 Use of unique compound PAV-073 and its stable derivatives may be available upon request by the Lead
476 Contact if sought for experimental purposes under a valid completed Materials Transfer Agreement.

477

478 **Chemical Synthesis** (see **Supplemental Figure 1** and **Supplemental Figure 3**)

479 **Synthesis of PAV-073**

480 A mixture of 3-hydroxy-4-methoxyacetophenone (16.6 g, 100 mmol), benzyl chloride (13.8 mL, 120
481 mmol), and anhydrous K₂CO₃ (20.7 g, 150 mmol) in DMF (100 mL) was heated at reflux for 5 h. The
482 reaction mixture was concentrated to dryness, the residue was redissolved in EtOAc (100 mL) and then
483 washed with 5% aqueous NaOH (3x30 mL). The organic layer was washed with brine (2x10 mL) and H₂O
484 (2x30 mL), dried (Na₂SO₄) and evaporated to a residue, which was purified by flash chromatography to
485 provide **1** (22.9 g, 90%). MS (m/z): 257 [M+H].

486 NaH (60 wt % in mineral oil, 1.95 g, 48.5 mmol) was suspended in THF (100 mL) and cooled to 0° C.

487 Triethylphosphonoacetate (9.6 mL, 48.5 mmol) was added dropwise and the reaction mixture was

488 stirred at 0° C. for 30 min. Then 3-benzyloxy-4-methoxy-acetophenone (**1**) (6.2 g, 24.2 mmol) was

489 dissolved in THF (0.1 ml/mmol) and added to the reaction mixture. The cooling bath was removed and

490 the mixture was stirred at 50° C. until full conversion was detected (TLC). The reaction mixture was

491 quenched by slow addition of H₂O (2 ml/mmol ketone), extracted with t-butyl methyl ether (3x3

492 ml/mmol) and the combined organic layers were dried (Na₂SO₄) and evaporated to give a residue,

493 which was purified by flash column chromatography to provide compound 2 (6.4 g, 81%). MS (m/z): 327
494 [M+H].

495 A mixture of ethyl ester (2) (6.4 g, 19.5 mmol) and alcoholic potassium hydroxide (4.0 g, 71 mmol KOH/
496 100 mL EtOH) was stirred at room temperature for 12 h. The solution was then concentrated to give a
497 residue, which was purified by flash column chromatography on silica gel to provide 3 (5.6 g, 96%). MS
498 (m/z): 299 [M+H].

499 A suspension of 3-(3-benzyloxy-4-methoxyphenyl)- 2-butenic acid (3) (5.6 g, 18.8 mmol), CuBr (270mg,
500 1.9 mmol) and tertiary butyl nitrite (8.9 mL, 37.6 mmol) in acetonitrile (50 mL) was stirred at 80° C. for
501 18 h. Reaction completion was monitored by TLC. After completion, the reaction mixture was cooled to
502 room temperature, solvent was removed under reduced pressure and the crude product was purified by
503 flash chromatography to yield compound 4 (3.9 g, 70%). MS (m/z): 300 [M+H].

504 To a solution of 3-(3-benzyloxy-4-methoxyphenyl)-l-nitro-2-butene (4) (3.9 g, 13.2 mmol) in 40 mL of
505 anhydrous THF under argon was slowly added a 2.0 M solution of LiAlH₄ in THF (40 mL, 80 mmol) and
506 the reaction mixture was heated at reflux for 2 h. The reaction mixture was cooled and excess reagent
507 was quenched by dropwise addition of H₂O and 15% aqueous NaOH. The reaction mixture was
508 extracted with CH₂Cl₂ (3x30 mL) and the combined organic layers were treated with 5% aqueous HCl.
509 The aqueous acid layer was then basified (5% aqueous NH₄OH, pH 9) and extracted with CH₂Cl₂. The
510 organic solution was washed with brine (2x30 mL) and H₂O (2x30 mL), dried (Na₂SO₄) and evaporated
511 to give compound (5) (2.3 g, 63%). MS (m/z): 272 [M+H].

512 To the stirred solution of (E)-3-(6-methyl-1,3-benzodioxol-5-yl)prop-2-enoic acid (8) [see synthesis
513 below] (140 mg, 0.68 mmol) and 2-(3-benzyloxy-4-methoxy-phenyl)propylamine (5) (185 mg, 0.68 mmol)
514 in DMF (2 mL) was added HATU (310 mg, 0.82 mmol) and diisopropylethylamine (351 mg, 0.473 mL,
515 15.0 mmol). The reaction mixture was stirred at room temperature for 1 h, diluted with EtOAc (50 mL),

516 washed with 10% citric acid, saturated aqueous solution of NaHCO₃, dried (Na₂SO₄), filtered and
517 evaporated to give a residue, which was purified by flash chromatography (ethyl acetate/hexanes) to
518 provide compound 6. Yield 11.4 mg (35% overall yield from nitrostyrene). MS (m/z): 460 [M+H].

519 A suspension of (E)-N-[2-(3-benzyloxy-4-methoxy-phenyl)-propyl]-3-(6-methyl-1,3-benzodioxol-5-yl)-
520 prop-2-enamide (6) (110 mg, 0.24 mmol) in dry acetonitrile (10 mL) was heated at reflux. Then
521 phosphorus oxychloride (400 mg, 0.24 mL, 2.6 mmol) was added drop wise and the reaction mixture
522 was heated at reflux for an additional 1 h. The solvent and reagent were evaporated under vacuum, the
523 organic layer was washed with water (2x10 mL). and evaporated in vacuo to give an oil, which was then
524 dissolved in ethanol (8 mL) and sodium borohydride (9.8 mg, 0.26 mmol) was added. The reaction
525 mixture was stirred at room temperature for 30 min and excess reagent was destroyed by dropwise
526 addition of 2 M HCl. The reaction mixture was basified with 2 M NaOH and ethanol was removed in
527 vacuo to give a residue, which was partitioned between water (10 mL) and chloroform (10 mL). The
528 organic layer was washed with water (2x10 mL), dried and evaporated to give a residue, which was
529 purified by column chromatography (dichloromethane/methanol) to give 6-nenzyloxy-7-methoxy-4-
530 methyl-1-[(E)-2-(6-methyl, 3-benzodioxol-5-yl)-vinyl]-1,2,3,4-tetrahydroisoquinoline (7) (10 mg, 10%).
531 MS (m/z): 444 [M+H].

532

533 **Synthesis of PAV-073 Photocrosslinker**

534 To 6-(tert-Butoxycarbonylamino)-2-(9H-fluoren-9-ylmethoxycarbonylamino)-hexanoic acid 9 [468mg
535 (1mmol)]a in a 40ml screw top vial was added 4N HCl in Dioxane (3ml). The vial was sealed and gently
536 agitated for 20min at room temperature. The mix was then rotary evaporated to dryness and the
537 residue placed on high vacuum overnight.

538 The dried residue was taken up into 4ml of DMF (anhydrous) and then sequentially treated with 3-(3-
539 Methyl diazirin-3-yl)-propanoic acid [128mg (1mmol)]^b, and DIEA [695ul (4mmol)]. With rapid stirring,
540 under Argon atmosphere, was added dropwise HATU [380mg (1mmol)] dissolved in 1ml of DMF. After
541 stirring for 30 min the mixture was quenched with 10ml of sat. NH₄Cl solution and then extracted 2 x
542 with 10ml of EtOAc.

543 The combined organic extracts were washed once with sat. NaCl, dried (Mg₂SO₄) and then rotary
544 evaporated to dryness. The residue was purified by flash chromatography, using a gradient of Ethyl
545 acetate and Hexane, affording 10 (293mg) in 61% yield.

546 To 6-benzyloxy-7-methoxy-4-methyl-1-[(E)-2-(6-methyl-1,3-benzodioxol-5-yl)vinyl]-1,2,3,4-
547 tetrahydroisoquinoline 7 [15mg (0.03 mmol)]^c in a 40ml screw top vial was added 4N HCl in Dioxane
548 (0.5ml). The vial was sealed and gently agitated for 20min at room temperature. The mix was then
549 rotary evaporated to dryness and the residue placed on high vacuum overnight.

550 The dried residue was taken up into 1ml of DMF (anhydrous) and then sequentially treated with 10
551 [14.5mg (0.03mmol)], and DIEA [32ul (0.18mmol)]. With rapid stirring, under Argon atmosphere, was
552 added dropwise HATU [14.6mg (0.038mmol)] dissolved in 300ul of DMF. After stirring for 30 min the
553 mixture was quenched with 5ml of sat. NH₄Cl solution and then extracted 2 x with 5ml of EtOAc.

554 The combined organic extracts were washed once with sat. NaCl, dried (Mg₂SO₄) and then rotary
555 evaporated to dryness. The residue was purified by flash chromatography, using a gradient of Ethyl
556 acetate and Hexane, affording 11 (28mg) in quant. yield.

557 To 11 [28mg (0.03 mmol)] in a 40ml screw top vial was added 50/50 Diethylamine / DMF (0.5ml). The
558 vial was sealed and gently agitated for 60min at room temperature. The mix was then rotary evaporated
559 to dryness and the residue placed on high vacuum overnight. The residue was triturated 2 x with 3ml of
560 Hexane to remove the Dibenzofulvene amine adduct. The residue was again briefly placed on high

561 vacuum to remove traces of Hexane. The dried residue was taken up into 1ml of DMF (anhydrous) and
562 then treated with Biotin-PEG2-NHS [15mg (0.03mmol)]d, and DIEA [16ul (0.09mmol)] and then purged
563 with Argon. After stirring overnight at room temperature, the mixture was rotary evaporated to dryness.
564 The residue was purified by reverse phase prep chromatography, using a gradient of 0.1% TFA water and
565 Acetonitrile, affording 12 (26mg) in 80% yield. Purity of all compounds were confirmed via LCMS.

566

567 **Method and Analysis Details**

568 ***In vitro studies***

569 **Stress granule aggregation in SH-SY5Y cells overexpressing TDP-43 SH-SY5Y cells:**

570 A TDP-43 cellular model was successfully generated by establishing stable cell-lines over-expressing
571 wild-type TDP-43 and M337V mutant TDP-43 and showing the display of stress granules, following
572 arsenite treatment. SH-SY5Y tet-on TDP-43 partial 3'-UTR (wt or M337V), 50.000 cells (DMEM/F12 + 1
573 µg/mL doxycycline) incubated on cover slips overnight. Cells were treated sodium arsenite at a final
574 concentration of 250 µM and incubated for 90 min. Cells were washed with 500 µL PBS. Cells were fixed
575 with 4% PFA in PBS pH 7.4 for 15 min at RT. Cells were washed with 500 µL PBS. Permeabilize/ block
576 cells with 5% milk powder, 1% BSA and 0.5 % saponin in PBS for 45 min @ RT. Add respective {TDP-43 C-
577 terminal domain Antibody (1:1000; Purchased from Proteintech), HuR (1:500; Purchased from Santa
578 Cruz} in 1% PBS and 0.5% saponine in PBS and incubated overnight at 4°C. Cells were washed 3 x with
579 500 µL PBS and incubated with secondary antibody at a dilution of 1:1000 AlexaFluor a-rabbit 594
580 (highly cross-adsorbed) (Thermo Fisher) or AlexaFluor a-mouse 488 (highly cross-adsorbed) (Thermo
581 Fisher). Cells were washed 3x with 500 µL PBS, then cells were washed with 500 µL dH2O. ProLong
582 Gold with DAPI embedding medium was used to fix cells on a glass slide. Image collection was done on a
583 Zeiss AxioImager 2 equipped with an Apotome using the following filtersets. For the automated image

584 analysis, each raw grayscale channel image was saved and analyzed independently. Each image set was
585 calibrated using the TDP-43 induced, sodium arsenite treated condition as a reference for exposure time
586 of the different channels.

587

588 **High-Content Imaging of Endogenous TDP-43 Stress Granule (SG):**

589 On day 1, seed 20,000 patient derived fibroblasts per well in a 24 well glass bottom plate or 6000 cells
590 per well in a 96 well plate. On day 2, sonicate compounds for 10 mins at 37oC before use. Add
591 compounds at the desired final concentration in fresh media to the respective wells. Add equivalent
592 amount of DMSO (LC-MS grade) to control wells. On Day 3, add sodium arsenite treatment- Add sodium
593 arsenite at a final concentration of 500uM. Incubate at 37oC for 60 mins. Wash 1X with PBS and fix cells
594 with 4% para formaldehyde (in PBS, prepared freshly, methanol free) for 15 mins at room temperature.
595 Wash 3X with PBS. Permeabilization and Blocking- Add 0.1% Triton-X for 10 mins for permeabilization
596 followed by 1 hour of blocking in 1% BSA. Immunostaining- Add the following primary antibodies in 1%
597 BSA (in PBS) and incubate it overnight at 4oC. Rabbit polyclonal TDP-43 C-terminal antibody (Proteintech
598 12892-1-AP)- 1:450; mouse monoclonal HuR antibody (Santa Cruz sc-5261)- 1:500. On day 4, wash 3X
599 with PBST (PBS + 0.1% Tween). The following secondary antibodies from Thermofisher Scientific (1:500)
600 in 1% BSA (in PBS) and keep it in dark for 1-2 hours at room temperature.
601 Alexa 594 anti-rabbit (highly cross-adsorbed); Alexa 488 anti-mouse (highly cross-adsorbed); Wash 3X
602 with PBST in dark. Add DAPI in PBS for nuclear staining. Imaging and Image analysis is done as explained
603 below. In brief, the immuno-stained cells were imaged with Nikon Ti inverted fluorescence microscope
604 having CSU-22 spinning disk confocal and EMCCD camera. Plan Apo objectives and NIS-Elements AR
605 software were used for image acquisition. At least 30-50 images per well is taken.

606 **Nucleocytoplasmic assay in FTD patient fibroblasts cells:**

607 Skin-derived fibroblasts cells from a sporadic Frontotemporal Degeneration (FTD) and ALS affected
608 individual acquired from the National Institute of Neurological Disorders and Stroke were grow in
609 HyClone DMEM High Glucose (GE Healthcare Life Sciences) supplemented with 15% FBS and 1% NEAA
610 (Non-Essential Amino Acids), at 37°C in an humidified atmosphere of 5% CO₂. On Day 1, seed 600 cells
611 per well in a 96 well glass bottom plate or 1200 cells per well in a 24 well glass bottom plate. Incubate
612 for 4 days, at 37°C in an humidified atmosphere of 5% CO₂. On day 5, sonicate compounds for 10
613 mins at 37°C before use. Add compounds at the desired final concentration in fresh media to the
614 respective wells. Add equivalent amount of DMSO (LC-MS grade) to control wells. Incubate for 4 days, at
615 37°C in a humidified atmosphere of 5% CO₂. On day 9, wash 2X with PBS. To fix add 4% para
616 formaldehyde (in PBS, prepared freshly, methanol free) for 15 mins at room temperature. Wash 3X with
617 PBS. Blocking and permeabilization- Add 1% BSA + 1% saponin (prepared in PBS) for 1 hour.
618 Immunostaining- Add the following primary antibodies in 1% BSA (in PBS) and incubate it overnight at
619 4°C. Rabbit polyclonal TDP-43 C-terminal antibody (Proteintech 12892-1-AP)- 1:350; mouse monoclonal
620 HuR antibody (Santa Cruz sc-5261)- 1:500. On day 10, wash 3X with PBST (PBS + 0.1% Tween). Add the
621 following secondary antibodies from Thermofisher Scientific (1:500) in 1% BSA (in PBS) and keep it in
622 dark for 1-2 hours at room temperature. Alexa 594 anti-rabbit (highly cross-adsorbed). Alexa 488 anti-
623 mouse (highly cross-adsorbed). Wash 3X with PBST in dark. Add DAPI in PBS for nuclear staining. The
624 immuno-stained cells are imaged with Nikon Ti inverted fluorescence microscope having CSU-22
625 spinning disk confocal and EMCCD camera. Plan Apo 20x/0.75 objective and NIS-Elements AR software
626 were used for image acquisition. At least 15 images per well are taken. The exposure times for TDP-43
627 and HuR must remain constant across one experiment. Each image acquired (in .nd format) is exported
628 into three individual channel images (for DAPI, TDP-43, HuR) in .tiff format. The images are analyzed by
629 the open source image analysis software Cell Profiler. The DAPI image is used to count the total number

630 of cells. The TDP-43 and HuR images are used to count the number of cells containing TDP-43 and/or
631 HuR nuclear staining.

632

633 **Automated Image Analysis and Machine Learning Tools:**

634 The immuno-stained cells were imaged with Nikon Ti inverted fluorescence microscope having CSU-22
635 spinning disk confocal and EMCCD camera. Plan Apo objectives and NIS-Elements AR software were
636 used for image acquisition. At least 30-50 images per well is taken. The exposure times for TDP-43 and
637 HuR must remain constant across one experiment. Each image acquired (in .nd format) is exported into
638 three individual channel images (for DAPI, TDP-43, HuR) in .tiff format. The images were analyzed by the
639 open source image analysis software CellProfiler 2.1.1 (offered by Broad Institute of Harvard and MIT-
640 www.cellprofiler.org). This software contains various modules which can be used to analyze images in
641 different ways. A Cell Profiler pipeline from a few of these modules was established to analyze our
642 images in order to quantify the number of cytoplasmic TDP-43 positive HuR stress granules. The outline
643 of the Cell Profiler pipeline: The three channel images are loaded and named DAPI, TDP-43 or HuR.
644 Identify primary objects- The DAPI image is used to identify the nucleus as an object. Identify secondary
645 objects- The nucleus is used to identify the cell boundary in the TDP-43 image by signal propagation.
646 Identify tertiary objects- Based on the nucleus and the cell boundary, cytoplasm is identified as an
647 object. Mask images- Using the cytoplasm object, the TDP-43 and HuR images are masked such that only
648 cytoplasmic signal will remain. Enhance features: Enhance the signal from TDP-43 and HuR aggregates in
649 cytoplasm for efficient identification of the aggregates. Identify primary objects- The TDP-43 aggregates
650 in the cytoplasm were identified from the TDP-43 image and HuR aggregates were identified from the
651 HuR image. Relate objects- This module enables the calculation of the number of TDP-43 aggregates
652 which has HuR and vice versa. Export to spreadsheet- This module exports all data into Excel sheets. The

653 final data has to be curated from the Excel sheets generated by Cell Profiler. The outlines for the
654 different objects (nucleus, cytoplasm, aggregates) must be saved to cross-check the proper
655 identification of objects once the analysis is done. At the beginning of analysis of an experiment, few
656 images (from DMSO wells) must be used as training set for Cell Profiler. Based on the training set, the
657 pipeline must be optimized with respect to intensity threshold, algorithm and size parameters for
658 correct identification of primary and secondary objects (nucleus, cytoplasm, aggregates). It is extremely
659 important to optimize this pipeline for every experiment. The pipeline must remain constant with
660 respect to aggregate identification for the analysis of all the images from the same experiment. Finally,
661 we calculate the number of TDP-43 positive HuR stress granules from the Excel sheets generated at the
662 end of Cell Profiler.

663

664 **HIV infectious virus assay**

665 MT-2 cells were preseeded in 96-well plates in 100 ul of complete RPMI. Multiple concentrations of
666 PAV-951 were serially diluted in DMSO then into an infection media prepared by diluting NL4-3 Rluc
667 virus stock to 400 IU/100 ul with complete RPMI, which was transferred onto the MT-2 cells with a final
668 MOI of 0.02 and final DMSO concentration of 1% in infected places. One well received DMSO only,
669 instead of PAV-951, and one well received medium only for normalization and background collection.
670 Cells were incubated at 37° C for 96 hours. 100ul of medium was removed and discarded and 10 ul of 15
671 uM EnduRen luciferase substrate was added to each well, followed by incubation for 1.5 hours at 37° C.
672 Plates were read on a luminescence plate reader. Bioluminescence intensity was read on a Synergy H1
673 BioTek plate reader. Averages and standard deviation for viral titer observed under different treatment
674 conditions were calculated in Microsoft Excel and graphed as the percent inhibition in PAV-951 treated
675 cells compared to untreated cells.

676 **Drug Resin affinity chromatography**

677 Mouse brains from wildtype or SOD1 mutant animals were homogenized in cold phosphate buffered
678 saline (PBS) (10mM sodium phosphate, 150 mM sodium chloride pH 7.4), then spun at 1,000 rpm for 10
679 minutes until pelleted. The PBS was decanted and the pellet resuspended in a low salt buffer (10mM
680 HEPES pH 7.6, 10mM NaCl, 1mM MgAc with 0.35% Tritonx100) then centrifuged at 10,000 rpm for 10
681 minutes at 4°C. The post-mitochondrial supernatant was removed and adjusted to a concentration of
682 approximately 10 mg/ml and equilibrated in a physiologic column buffer (50 mM Hepes ph 7.6, 100 mM
683 KAc, 6 mM MgAc, 1 mM EDTA, 4mM TGA). In some conditions, the extract was supplemented with an
684 energy cocktail (to a final concentration of 1mM rATP, 1mM rGTP, 1mM rCTP, 1mM rUTP, and 5 ug/mL
685 creatine kinase). 30 ul or 230 ul of extract was then incubated for one hour at either 4° C or 22° C
686 degrees on 30 ul of affigel resin coupled to THIQ compound or a 4% agarose matrix (control). The input
687 material was collected and the resin was then washed with 3 ml column buffer. The resins were eluted
688 for 2 hours then overnight at 22°C then 4°C in 100ul column buffer containing 100uM of the cognate
689 compound. Eluates were run on western blot or sent for mass spectrometry for analysis.

690

691 **Chemical photocrosslinking**

692 Extract from mouse brain and PDFs grown in minimum essential media were prepared as above then
693 adjusted to a protein concentration of approximately 3 mg/ml in column buffer containing 0.01% triton.
694 1% DMSO or 100uM PAV-073 was added to 6ul of extract, then 3uM of PAV-073 photocrosslinker or a
695 negative control crosslinker (comprising of the biotin and diazine moieties without compound) were
696 added. The extract was incubated for 20 minutes then exposed to UV at 365nm wavelength for 10
697 minutes then left on ice for one hour. After crosslinking, samples were divided in two 20 ul aliquots and
698 one set was denatured by adding 20 uL of column buffer 4ul of 10% SDS, 0.5 ul 1M DTT, and boiling for 5

699 minutes. Both native and denatured aliquots were then diluted in 800 ul column buffer containing 0.1%
700 triton. 5 ul of magnetic streptavidin beads (Pierce) were added to all samples and mixed for one hour at
701 room temperature to capture all biotinylated proteins and co-associated proteins. Samples were placed
702 on a magnetic rack to hold the beads in place and washed three times with 800 ul of column buffer
703 containing 0.1% triton. After washing, beads were resuspended in 80 ul of gel loading buffer containing
704 SDS and analyzed by western blot or blot for affinity purified streptavidin. Samples were analyzed by
705 western blot.

706

707 **Western blotting**

708 SDS/PAGE gels were transferred in Towbin buffer (25mM Tris, 192mM glycine, 20% w/v methanol) to
709 polyvinylidene fluoride membrane, blocked in 1% bovine serum albumin (BSA) in PBS, incubated
710 overnight at 4°C in a 1:1,000 dilution of 100ug/mL affinity-purified primary IGG to PDI in 1% BSA in PBS
711 containing 0.1% Tween-20 (PBST). Membranes were then washed twice in PBST and incubated for two
712 hours at room temperature in a 1:5000 dilution of secondary anti-rabbit or anti-mouse antibody coupled
713 to alkaline phosphatase in PBST. Membranes were washed two more times in PBST then incubated in a
714 developer solution prepared from 100 uL of 7.5 mg/mL 5-bromo-4-chloro-3-indolyl phosphate dissolved
715 in 60% dimethyl formamide (DMF) in water and 100ul of 15 mg/ml nitro blue tetrazolium dissolved in
716 70% DMF in water, adjusted to 50mL with 0.1 Tris (pH 9.5) and 0.1 mM magnesium chloride.
717 Membranes were scanned and the integrated density of protein band was measured on ImageJ.
718 Averages and the standard deviation between repeated experiments were calculated and plotted on
719 Microsoft Excel.

720

721

722 **Tandem mass spectrometry**

723 Samples were processed by SDS PAGE using a 10% Bis-tris NuPAGE gel with the 2-(N-
724 morpholino)ethanesulfonic acid buffer system. The mobility region was excised and washed with 25 mM
725 ammonium bicarbonate followed by 15mM acetonitrile. Samples were reduced with 10 mM
726 dithiothreitol and 60° C followed by alkylation with 50 mM iodoacetamide at room temperature.
727 Samples were then digested with trypsin (Promega) overnight (18 hours) at 37° C then quenched with
728 formic acid and desalted using an Empore SD plate. Half of each digested sample was analyzed by LC-
729 MS/MS with a Waters NanoAcquity HPLC system interfaced to a ThermoFisher Q Exactive. Peptides
730 were loaded on a trapping column and eluted over a 75 uM analytical column at 350 nL/min packed
731 with Luna C18 resin (Phenomenex). The mass spectrometer was operated in a data dependent mode,
732 with the Orbitrap operating at 60,000 FWHM and 15,000 FWHM for MS and MS/MS respectively. The
733 fifteen most abundant ions were selected for MS/MS.

734 Data was searched using a local copy of Mascot (Matrix Science) with the following parameters: Enzyme:
735 Trypsin/P; Database: SwissProt Human (conducted forward and reverse plus common contaminants);
736 Fixed modification: Carbamidomethyl (C) Variable modifications: Oxidation (M), Acetyl (N-term), Pyro-
737 Glu (N-term Q), Deamidation (N/Q) Mass values: Monoisotopic; Peptide Mass Tolerance: 10 ppm;
738 Fragment Mass Tolerance: 0.02 Da; Max Missed Cleavages: 2. The data was analyzed by spectral count
739 methods.

740

741

742

743

744 ***In vivo studies***

745 **Transgenic Human TDP-43 mutant *C. elegans***

746 MosSCI homologous-recombination transgenesis was used to create an unc-47p::hTDP-43::unc-54utr or
747 unc-47p::hTDP-43(mutant M337V)::unc-54utr transgenic. Transgenesis requires MOSSCI plasmid
748 inserted with unc-47p::hTDP-43::unc-54utr or unc-47p::hTDP-43(mutant M337V)::unc-54utr. Injection
749 mix used Standard MosSCI mix. Injections were performed into mos1 ttTi5605 background strain.
750 Extrachromosomal array lines were isolated. Crawling transgenics screened as non-red homozygotes
751 were verified by PCR for insertion/replacement at target locus resulting verified single copy integrated
752 strains. Transgenic *C. elegans* expressing the human TDP-43 wild-type or mutant TDP-43 M337V animal
753 model that mimic aspects of TDP-43 specific ALS disease pathogenesis were generated. The transgenic
754 *C. elegans* had a single copy of the human TDP-43 gene integrated into its genome. The expression is
755 controlled by an unc-47 promoter and hence human TDP-43 protein was specifically expressed only in
756 the *C. elegans* motor neurons. *C. elegans* studies were also performed with worms transgenic for the
757 hTDP-43 (A315T) mutation using methods described in detail elsewhere(23,45).

758

759 **Age-synchronizing *C. elegans***

760 Filtered deionized water is used to wash worms off of plates and into 15ml tubes which are centrifuged
761 at 1200 rpm for 2 minutes and repeated twice. The supernatant is aspirated and 5ml of NaOH + bleach
762 solution added. This is vortexed gently about every minute and monitored by microscope. The adults
763 worms split open and their eggs are released. The adult worms also dissolve into the solution. Once all
764 adult worms have dissolved, the reaction is neutralized by adding 5 ml of M9 buffer followed by three
765 rounds of centrifugation at 2500 rpm for 2 minutes. After one wash with 10 ml of water, all but about
766 200- 1000ul is aspirated from the 15ml tube and the remaining pellet will be re-suspended in leftover

767 water. This are dropped onto the plates evenly, thus ensuring that the larva that hatches have enough
768 food while they grow over the next few days. Plates will be stored at 20°C.

769

770 **Swimming-induced Paralysis (SWIP) Assay**

771 The age-synchronized worms are washed off NGM plates in S-media that contains 0.02% Triton. This
772 allows for a more consistent number of worms while pipetting, as less worms stick to the plastic pipette
773 tips. The volume is adjusted with S-media until there would be 60-70 worms per 20ul. Worms are scored
774 as paralyzed if their body cannot make a bending “S” movement. Paralyzed worms can often still make
775 small movements with their head or tail. Videos are captured using a Lumenera Infinity 3s camera fitted
776 to a Nikon TE300 microscope at 2x magnification and recorded to ImageJ. In some experiments videos
777 are captured using Phylumtech's Wormtracker machine. The videos will be analyzed using ImageJ *C.*
778 *elegans* motility analysis software. Level of activity will be denoted based on improvement in swimming
779 induced paralysis (SWIP) in human TDP-43 transgenic *C. elegans* disease model. The automation data
780 measuring paralysis will measure average body bends per second of a population. Improvement in SWIP
781 from control in the population of worms will also be observed.

782

783 **Drosophila Drug feeding assay**

784 Melt cornmeal-molasses-yeast fly food was mixed with certain concentrations of compound at high
785 temperature and cooled to RT. DMSO was used as the vehicle control. Parent flies were crossed on food
786 supplemented with drugs and the offspring were raised on the same food. Adult flies were aged on the
787 drug-containing food for 15 days before analyzing their eye morphology. For quantification of outer eye
788 morphological defects, ten flies were quantified.

789

790 **SODG93A Mouse Efficacy Study**

791 Wildtype and SODG93A mutant mice were grown for 5 weeks, then given daily IP doses with vehicle,
792 compound T18, or compound T20 for another 5 weeks. Weight and serum pNHF were tracked during
793 the study.

794

795 Abbreviations

796 Amyotrophic lateral sclerosis (ALS)

797 Adenosine triphosphate (rATP)

798 Bovine serum albumin (BSA)

799 Cell-free protein synthesis and assembly (CFPSA)

800 Cytidine triphosphate (rCTP)

801 Energy-dependent drug resin affinity chromatography (eDRAC)

802 Fronto-temporal dementia (FTD)

803 Guanosine triphosphate (rGTP)

804 Human immunodeficiency virus (HIV)

805 Intraperitoneal (IP)

806 Liquid chromatography (LC)

807 Mass spectrometry (MS)

808 Milliliter (mL)

809 Millimolar (mM)

810 Milligram (mg)

811 Patient-derived fibroblasts (PDF)

- 812 Phosphate buffered saline (PBS)
- 813 Phosphorylated neurofilament heavy chain (pNFH)
- 814 Protein disulfide isomerase (PDI)
- 815 Streptavidin precipitation (SAP)
- 816 Stress granule (SG)
- 817 Structure-activity relationship (SAR)
- 818 Swimming-induced paralysis (SWIP)
- 819 Tandem mass spectrometry (MS-MS)
- 820 Tetrahydroisoquinolone (THIQ)
- 821 Transactive DNA-binding protein of 43 kDa (TDP-43)
- 822 Uridine triphosphate (UTP)

823

824 Acknowledgments

825 We thank the Target ALS postmortem tissue core for providing blinded ALS and healthy tissues. Funding
826 for these studies was provided by Prosetta Biosciences.

827

828 Competing interests

829 VRL is CEO of Prosetta Biosciences

830

831

832

833 References

- 834 1. Gandhi J, Antonelli AC, Afridi A, Vatsia S, Joshi G, Romanov V, et al. Protein misfolding and
835 aggregation in neurodegenerative diseases: a review of pathogenesis, novel detection strategies,
836 and potential therapeutics. *Rev Neurosci*. 2019 May 27;30(4):339–58.
- 837 2. Yerbury JJ, Ooi L, Dillin A, Saunders DN, Hatters DM, Beart PM, et al. Walking the tightrope:
838 proteostasis and neurodegenerative disease. *J Neurochem*. 2016 May;137(4):489–505.
- 839 3. Blokhuis AM, Groen EJN, Koppers M, van den Berg LH, Pasterkamp RJ. Protein aggregation in
840 amyotrophic lateral sclerosis. *Acta Neuropathol (Berl)*. 2013 Jun;125(6):777–94.
- 841 4. Gordon DE, Hiatt J, Bouhaddou M, Rezelj VV, Ulferts S, Braberg H, et al. Comparative host-
842 coronavirus protein interaction networks reveal pan-viral disease mechanisms. *Science*. 2020 Dec
843 4;370(6521):eabe9403.
- 844 5. Chou CC, Zhang Y, Umoh ME, Vaughan SW, Lorenzini I, Liu F, et al. TDP-43 pathology disrupts nuclear
845 pore complexes and nucleocytoplasmic transport in ALS/FTD. *Nat Neurosci*. 2018 Feb;21(2):228–39.
- 846 6. Gendron TF, Josephs KA, Petrucelli L. Review: Transactive response DNA-binding protein 43 (TDP-43):
847 mechanisms of neurodegeneration. *Neuropathol Appl Neurobiol*. 2010 Apr;36(2):97–112.
- 848 7. Prasad A, Bharathi V, Sivalingam V, Girdhar A, Patel BK. Molecular Mechanisms of TDP-43 Misfolding
849 and Pathology in Amyotrophic Lateral Sclerosis. *Front Mol Neurosci*. 2019 Feb 14;12:25.
- 850 8. Suk TR, Rousseaux MWC. The role of TDP-43 mislocalization in amyotrophic lateral sclerosis. *Mol*
851 *Neurodegener*. 2020 Dec;15(1):45.
- 852 9. Igaz LM, Kwong LK, Xu Y, Truax AC, Uryu K, Neumann M, et al. Enrichment of C-Terminal Fragments in
853 TAR DNA-Binding Protein-43 Cytoplasmic Inclusions in Brain but not in Spinal Cord of Frontotemporal
854 Lobar Degeneration and Amyotrophic Lateral Sclerosis. *Am J Pathol*. 2008 Jul;173(1):182–94.
- 855 10. Neumann M, Sampathu DM, Kwong LK, Truax AC, Micsenyi MC, Chou TT, et al. Ubiquitinated
856 TDP-43 in Frontotemporal Lobar Degeneration and Amyotrophic Lateral Sclerosis. *Science*. 2006 Oct
857 6;314(5796):130–3.
- 858 11. Baradaran-Heravi Y, Van Broeckhoven C, van der Zee J. Stress granule mediated protein
859 aggregation and underlying gene defects in the FTD-ALS spectrum. *Neurobiol Dis*. 2020
860 Feb;134:104639.
- 861 12. Li YR, King OD, Shorter J, Gitler AD. Stress granules as crucibles of ALS pathogenesis. *J Cell Biol*.
862 2013 Apr 29;201(3):361–72.
- 863 13. Chiò A, Logroscino G, Hardiman O, Swingler R, Mitchell D, Beghi E, et al. Prognostic factors in
864 ALS: A critical review. *Amyotroph Lateral Scler*. 2009 Jan;10(5–6):310–23.
- 865 14. Dharmadasa T. Cortical Excitability across the ALS Clinical Motor Phenotypes. *Brain Sci*. 2021
866 May 28;11(6):715.

- 867 15. Grad LI, Rouleau GA, Ravits J, Cashman NR. Clinical Spectrum of Amyotrophic Lateral Sclerosis
868 (ALS). *Cold Spring Harb Perspect Med*. 2017 Aug;7(8):a024117.
- 869 16. Gros-Louis F, Gaspar C, Rouleau GA. Genetics of familial and sporadic amyotrophic lateral
870 sclerosis. *Biochim Biophys Acta BBA - Mol Basis Dis*. 2006 Nov;1762(11–12):956–72.
- 871 17. Chia R, Chiò A, Traynor BJ. Novel genes associated with amyotrophic lateral sclerosis: diagnostic
872 and clinical implications. *Lancet Neurol*. 2018 Jan;17(1):94–102.
- 873 18. Ghasemi M, Brown RH. Genetics of Amyotrophic Lateral Sclerosis. *Cold Spring Harb Perspect
874 Med*. 2018 May;8(5):a024125.
- 875 19. Dervishi I, Gozutok O, Murnan K, Gautam M, Heller D, Bigio E, et al. Protein-protein interactions
876 reveal key canonical pathways, upstream regulators, interactome domains, and novel targets in ALS.
877 *Sci Rep*. 2018 Oct 3;8(1):14732.
- 878 20. Zufiría M, Gil-Bea FJ, Fernández-Torrón R, Poza JJ, Muñoz-Blanco JL, Rojas-García R, et al. ALS: A
879 bucket of genes, environment, metabolism and unknown ingredients. *Prog Neurobiol*. 2016
880 Jul;142:104–29.
- 881 21. Cox PA, Kostrzewa RM, Guillemin GJ. BMAA and Neurodegenerative Illness. *Neurotox Res*. 2018
882 Jan;33(1):178–83.
- 883 22. Hobert O. Neurogenesis in the nematode *Caenorhabditis elegans*. *WormBook* [Internet]. 2010
884 Oct 4 [cited 2023 Jan 30]; Available from:
885 http://www.wormbook.org/chapters/www_specnervsys.2/neurogenesis.html
- 886 23. Vaccaro A, Tauffenberger A, Aggad D, Rouleau G, Drapeau P, Parker JA. Mutant TDP-43 and FUS
887 Cause Age-Dependent Paralysis and Neurodegeneration in *C. elegans*. Petrucelli L, editor. *PLoS ONE*.
888 2012 Feb 21;7(2):e31321.
- 889 24. Raji JI, Potter CJ. The number of neurons in *Drosophila* and mosquito brains. Louis M, editor.
890 *PLOS ONE*. 2021 May 14;16(5):e0250381.
- 891 25. Zhang K, Donnelly CJ, Haeusler AR, Grima JC, Machamer JB, Steinwald P, et al. The C9orf72
892 repeat expansion disrupts nucleocytoplasmic transport. *Nature*. 2015 Sep 3;525(7567):56–61.
- 893 26. De Giorgio F, Maduro C, Fisher EMC, Acevedo-Arozena A. Transgenic and physiological mouse
894 models give insights into different aspects of amyotrophic lateral sclerosis. *Dis Model Mech*. 2019 Jan
895 1;12(1):dmm037424.
- 896 27. Lingappa VR, Hurt CR, Garvey E. Capsid assembly as a point of intervention for novel anti-viral
897 therapeutics. *Curr Pharm Biotechnol*. 2013;14(5):513–23.
- 898 28. Zlotnick A, Mukhopadhyay S. Virus assembly, allostery and antivirals. *Trends Microbiol*. 2011
899 Jan;19(1):14–23.

- 900 29. Lingappa UF, Wu X, Macieik A, Yu SF, Atuegbu A, Corpuz M, et al. Host–rabies virus protein–
901 protein interactions as druggable antiviral targets. *Proc Natl Acad Sci [Internet]*. 2013 Mar 5 [cited
902 2022 May 13];110(10). Available from: <https://pnas.org/doi/full/10.1073/pnas.1210198110>
- 903 30. Reed JC, Solas D, Kitaygorodskyy A, Freeman B, Ressler DTB, Phuong DJ, et al. Identification of an
904 Antiretroviral Small Molecule That Appears To Be a Host-Targeting Inhibitor of HIV-1 Assembly.
905 Simon V, editor. *J Virol*. 2021 Jan 13;95(3):e00883-20.
- 906 31. Lingappa JR, Reed JC, Tanaka M, Chutiraka K, Robinson BA. How HIV-1 Gag assembles in cells:
907 Putting together pieces of the puzzle. *Virus Res*. 2014 Nov 26;193:89–107.
- 908 32. Müller-Schiffmann A, Trossbach SV, Lingappa VR, Korth C. Viruses as ‘Truffle Hounds’: Molecular
909 Tools for Untangling Brain Cellular Pathology. *Trends Neurosci*. 2021 May;44(5):352–65.
- 910 33. Lingappa JR, Martin RL, Wong ML, Ganem D, Welch WJ, Lingappa VR. A eukaryotic cytosolic
911 chaperonin is associated with a high molecular weight intermediate in the assembly of hepatitis B
912 virus capsid, a multimeric particle. *J Cell Biol*. 1994 Apr;125(1):99–111.
- 913 34. Lingappa JR, Hill RL, Wong ML, Hegde RS. A multistep, ATP-dependent pathway for assembly of
914 human immunodeficiency virus capsids in a cell-free system. *J Cell Biol*. 1997 Feb 10;136(3):567–81.
- 915 35. Lingappa AF, Akintunde O, Ewald C, Froehlich M, Ziari N, Yu SF, et al. Small Molecule Assembly
916 Modulators with Pan-Cancer Therapeutic Efficacy [Internet]. *Cancer Biology*; 2022 Sep [cited 2023 Jan
917 19]. Available from: <http://biorxiv.org/lookup/doi/10.1101/2022.09.28.509937>
- 918 36. Müller-Schiffmann A, Michon M, Lingappa AF, Yu SF, Du L, Deiter F, et al. A Pan-respiratory
919 Antiviral Chemotype Targeting a Transient Host Multiprotein Complex. *BioRxiv Prepr Serv Biol*. 2022
920 Jul 19;2021.01.17.426875.
- 921 37. Müller-Schiffmann A, Torres F, Kitaygorodskyy A, Ramani A, Alatza A, Tschirner SK, et al.
922 Oxidized MIF is an Alzheimer’s Disease drug target relaying external risk factors to tau pathology
923 [Internet]. *Neuroscience*; 2023 Jan [cited 2023 Apr 5]. Available from:
924 <http://biorxiv.org/lookup/doi/10.1101/2021.09.11.459903>
- 925 38. Marreiros R, Müller-Schiffmann A, Bader V, Selvarajah S, Dey D, Lingappa VR, et al. Viral capsid
926 assembly as a model for protein aggregation diseases: Active processes catalyzed by cellular assembly
927 machines comprising novel drug targets. *Virus Res*. 2015 Sep;207:155–64.
- 928 39. Cocoros NM, Svensson E, Szépligeti SK, Vestergaard SV, Szentkúti P, Thomsen RW, et al. Long-
929 term Risk of Parkinson Disease Following Influenza and Other Infections. *JAMA Neurol*. 2021 Dec
930 1;78(12):1461.
- 931 40. Li Puma DD, Piacentini R, Leone L, Gironi K, Marcocci ME, De Chiara G, et al. Herpes Simplex
932 Virus Type-1 Infection Impairs Adult Hippocampal Neurogenesis via Amyloid- β Protein Accumulation.
933 *Stem Cells*. 2019 Nov 1;37(11):1467–80.
- 934 41. Mancuso R, Sicurella M, Agostini S, Marconi P, Clerici M. Herpes simplex virus type 1 and
935 Alzheimer’s disease: link and potential impact on treatment. *Expert Rev Anti Infect Ther*. 2019 Sep
936 2;17(9):715–31.

- 937 42. Li W, Lee MH, Henderson L, Tyagi R, Bachani M, Steiner J, et al. Human endogenous retrovirus-K
938 contributes to motor neuron disease. *Sci Transl Med* [Internet]. 2015 Sep 30 [cited 2022 Jun
939 23];7(307). Available from: <https://www.science.org/doi/10.1126/scitranslmed.aac8201>
- 940 43. Campioni MR, Finkbeiner S. Going Retro: Ancient Viral Origins of Cognition. *Neuron*. 2015
941 Apr;86(2):346–8.
- 942 44. Reed JC, Westergreen N, Barajas BC, Ressler DTB, Phuong DJ, Swain JV, et al. Formation of RNA
943 Granule-Derived Capsid Assembly Intermediates Appears To Be Conserved between Human
944 Immunodeficiency Virus Type 1 and the Nonprimate Lentivirus Feline Immunodeficiency Virus. *J Virol*.
945 2018 01;92(9).
- 946 45. Patten SA, Aggad D, Martinez J, Tremblay E, Petrillo J, Armstrong GA, et al. Neuroleptics as
947 therapeutic compounds stabilizing neuromuscular transmission in amyotrophic lateral sclerosis. *JCI*
948 *Insight*. 2017 Nov 16;2(22).
- 949 46. Tanaka A. Identification of the Specific Binding Proteins of Bioactive Small Compound Using
950 Affinity Resins. In: Koga H, editor. *Reverse Chemical Genetics* [Internet]. Totowa, NJ: Humana Press;
951 2009 [cited 2022 Jul 7]. p. 181–95. (Methods in Molecular Biology; vol. 577). Available from:
952 http://link.springer.com/10.1007/978-1-60761-232-2_14
- 953 47. Andreas Müller-Schiffmann, Felix Torres, Anatolly Kitaygorodskyy, Anand Ramani, Argyro Alatzta,
954 Sarah K. Tschirner, et al. Oxidized MIF is an Alzheimer’s Disease drug target relaying external risk
955 factors to tau pathology. *bioRxiv*. 2023 Jan 1;2021.09.11.459903.
- 956 48. Jia H, Liang Z, Zhang X, Wang J, Xu W, Qian H. 14-3-3 proteins: an important regulator of
957 autophagy in diseases. *Am J Transl Res*. 2017;9(11):4738–46.
- 958 49. Iyengar S, Farnham PJ. KAP1 protein: an enigmatic master regulator of the genome. *J Biol Chem*.
959 2011 Jul 29;286(30):26267–76.
- 960 50. Chiu J, Hogg PJ. Allosteric disulfides: Sophisticated molecular structures enabling flexible protein
961 regulation. *J Biol Chem*. 2019 Feb 22;294(8):2949–60.
- 962 51. Hotchkiss KA, Matthias LJ, Hogg PJ. Exposure of the cryptic Arg-Gly-Asp sequence in
963 thrombospondin-1 by protein disulfide isomerase. *Biochim Biophys Acta*. 1998 Nov 10;1388(2):478–
964 88.
- 965 52. Hotchkiss KA, Chesterman CN, Hogg PJ. Catalysis of disulfide isomerization in thrombospondin 1
966 by protein disulfide isomerase. *Biochemistry*. 1996 Jul 30;35(30):9761–7.
- 967 53. Schmidt B, Ho L, Hogg PJ. Allosteric disulfide bonds. *Biochemistry*. 2006 Jun 20;45(24):7429–33.
- 968 54. Gonzalez-Perez P, Woehlbier U, Chian RJ, Sapp P, Rouleau GA, Leblond CS, et al. Identification of
969 rare protein disulfide isomerase gene variants in amyotrophic lateral sclerosis patients. *Gene*. 2015
970 Jul 25;566(2):158–65.
- 971 55. Walker AK. Protein disulfide isomerase and the endoplasmic reticulum in amyotrophic lateral
972 sclerosis. *J Neurosci Off J Soc Neurosci*. 2010 Mar 17;30(11):3865–7.

- 973 56. Woehlbier U, Colombo A, Saaranen MJ, Pérez V, Ojeda J, Bustos FJ, et al. ALS-linked protein
974 disulfide isomerase variants cause motor dysfunction. *EMBO J*. 2016 Apr 15;35(8):845–65.
- 975 57. Parakh S, Perri ER, Vidal M, Sultana J, Shadfar S, Mehta P, et al. Protein disulphide isomerase
976 (PDI) is protective against amyotrophic lateral sclerosis (ALS)-related mutant Fused in Sarcoma (FUS)
977 in in vitro models. *Sci Rep*. 2021 Sep 2;11(1):17557.
- 978 58. Walker AK, Farg MA, Bye CR, McLean CA, Horne MK, Atkin JD. Protein disulphide isomerase
979 protects against protein aggregation and is S-nitrosylated in amyotrophic lateral sclerosis. *Brain J*
980 *Neurol*. 2010 Jan;133(Pt 1):105–16.
- 981 59. Yang YS, Harel NY, Strittmatter SM. Reticulon-4A (Nogo-A) redistributes protein disulfide
982 isomerase to protect mice from SOD1-dependent amyotrophic lateral sclerosis. *J Neurosci Off J Soc*
983 *Neurosci*. 2009 Nov 4;29(44):13850–9.
- 984 60. Copley SD. Moonlighting is mainstream: paradigm adjustment required. *BioEssays News Rev*
985 *Mol Cell Dev Biol*. 2012 Jul;34(7):578–88.
- 986 61. Jeffery CJ. Multitalented actors inside and outside the cell: recent discoveries add to the number
987 of moonlighting proteins. *Biochem Soc Trans*. 2019 20;47(6):1941–8.
- 988 62. Fenton AW. Allosteric: an illustrated definition for the ‘second secret of life.’ *Trends Biochem Sci*.
989 2008 Sep;33(9):420–5.
- 990